T follicular helper cell profiles differ by malaria antigen and for children compared to adults

Catherine S. Forconi[1], Christina Nixon[2], Hannah W. Wu[2], Boaz Odwar[3], Sunthorn Pond-Tor[2], John M. Ong'echa[3], Jonathan Kurtis[2] and Ann M. Moormann[1]*

[1]Division of Infectious Diseases and Immunology, Department of Medicine, University of Massachusetts Chan Medical School, Worcester, MA, USA

[2]Department of Pathology and Laboratory Medicine, Brown University, Providence, RI, USA

[3]Center for Global Health Research, Kenya Medical Research Institute, Kisumu, Kenya

*Corresponding author

Ann Moormann, PhD, MPH, FAAS, FASTMH

Department of Medicine

Division of Infectious Diseases and Immunology

University of Massachusetts Chan Medical School

364 Plantation Street, LRB 313

Worcester, MA 01605 USA

Office: 508-856-8826 (VoIP)

Lab: 508-856-4562

Email: ann.moormann@umassmed.edu

Abstract

Background

Circulating T-follicular helper (cT_{FH}) cells have the potential to provide an additional correlate of protection against *Plasmodium falciparum* (*Pf)* as they are essential to promote B cell production of long-lasting antibodies. Assessing the specificity of cT_{FH} subsets to individual malaria antigens is vital to understanding the variation observed in antibody responses and identifying promising malaria vaccine candidates.

Methods

Using spectral flow cytometry and unbiased clustering analysis we assessed antigen-specific cT_{FH} cell recall responses *in vitro* to malaria vaccine candidates *Pf*SEA-1A and *Pf*GARP within a cross-section of children and adults living in a malaria holoendemic region of western Kenya.

Findings

In children, a broad array of cT_{FH} subsets (defined by cytokine and transcription factor expression) were reactive to both malaria antigens, *Pf*SEA-1A and *Pf*GARP, while adults had a narrow profile centering on $cT_{FH}17$- and $cT_{FH}1/17$-like subsets following stimulation with *Pf*GARP only.

Interpretation

Because $T_{FH}17$ cells are involved in the maintenance of memory antibody responses within the context of parasitic infections, our results suggest that *Pf*GARP might generate longer lived antibody responses compared to *Pf*SEA-1A. These findings have intriguing implications for evaluating malaria vaccine candidates as they highlight the importance of including cT_{FH} profiles when assessing interdependent correlates of protective immunity.

Keywords T-follicular-helper, *Pf*-malaria, vaccine candidates, Kenya

Introduction

Despite progress made to reduce the global malaria burden, *Plasmodium falciparum* (*Pf*) remains one of the leading causes of mortality among children under 5 years of age.(Geneva: World Health Organization, 2022) Unfortunately, progress has been impeded by a plateau in malaria control since 2015. Anti-malarial drug resistance,(Aydemir et al., 2018; Taylor and Juliano, 2014) and unprecedented logistical challenges during the COVID-19 pandemic that dramatically impacted the distribution of insecticide-impregnated mosquito nets led to an increase in malaria cases in children under 5 years of age from 17.6 million in 2015 to 19.2 million in 2021 in East and Southern African countries,(Geneva: World Health Organization, 2022; Ippolito et al., 2021) thus, contributing to reinvigorated prioritization of malaria vaccine initiatives.

After 30 years of development, the first malaria vaccine - RTS,S/AS01E - was approved by the World Health Organization in 2021 for use in children residing in malaria endemic regions. However, the limited efficacy of RTS,S,(RTS,S Clinical Trials Partnership, 2015) particularly against severe malaria(RTS,S Clinical Trials Partnership, 2015) has motivated the search for additional vaccine candidate antigens including blood-stage *Pf*-schizont egress antigen-1 (*Pf*SEA-1A)(Raj et al., 2014) and *Pf*-glutamic acid-rich protein (*Pf*GARP).(Raj et al., 2020) Antibodies against *Pf*SEA-1A correlate with significantly lower parasite densities in Kenyan adults and adolescents, and substantially reduce schizont replication *in vitro*.(Nixon et al., 2017; Raj et al., 2014) Whereas *Pf*GARP-specific antibodies kill trophozoite-infected erythrocytes in culture and confer partial protection against *Pf*-challenge in vaccinated non-human primates.(Raj et al., 2020) The presence of antibodies against *Pf*GARP was associated with a 2-fold-lower parasite density in Kenyan adults and adolescents.(Raj et al., 2020) Due to the complexity of the parasites' life cycle, there is consensus that a multi-valent vaccine would prove to be more efficacious(Holder, 1999).

However, determining which vaccine candidate antigens hold the most promise for inclusion in next-generation malaria vaccines remains a challenge.

Many pathogens and vaccines engender protective antibody responses after a single or few exposures(Amanna et al., 2007) characterized by the production of long-lived plasma cells and memory B cells.(Tarlinton and Good-Jacobson, 2013) Affinity maturation takes place in the germinal center (GC) where not only antigen-specific $CD4^{pos}$ T-follicular helper (T_{FH}) cells are required to provide cellular (CD40L) and molecular (IL21, IL4, IL13) signals to trigger B cell proliferation, promote GC maintenance and plasmablast differentiation, but where higher affinity B cells also out-compete B cells with lower affinity for T_{FH} help.(Crotty, 2019, 2014) T_{FH} cells are defined by the expression of a combination of markers, starting with chemokine receptor CXCR5 which directs $CD4^{pos}$ T cells from the T cell zone to engagement with follicular B cells.(Breitfeld et al., 2000; Crotty, 2011) Once antigen-experienced T_{FH} cells leave the GC, they become circulating T_{FH} (cT_{FH}) cells, and correlate with the generation of long-lasting antibody responses. Expression profiles of CCR6 and CXCR3 categorize cT_{FH} subsets as follow: $cT_{FH}1$ ($CCR6^{neg}CXCR3^{pos}$), $cT_{FH}2$ ($CCR6^{neg}CXCR3^{neg}$) and $cT_{FH}17$ ($CCR6^{pos}CXCR3^{neg}$)(Schmitt et al., 2014); whereas the expression of PD-1, ICOS, CD127 and CCR7 define their functional status: quiescent/central memory cT_{FH} ($CCR7^{high}PD\text{-}1^{neg}ICOS^{neg}CD127^{pos}$) or activated/effector memory cT_{FH} ($CCR7^{low}PD\text{-}1^{pos}ICOS^{pos}CD127^{low/neg}$).(Dunham et al., 2008; Gong et al., 2019; Schmitt et al., 2014) In addition, transcription factors (i.e., Bcl6 and cMAF) and cytokines (i.e., IFN□, IL-4, and IL-21) are crucial to further characterizing the role of each cT_{FH} subset within the context of their interactions with B cells to promote antibody production.(Andris et al., 2017; Bélanger and Crotty, 2016; Olatunde et al., 2021; Seth and Craft, 2019) Bcl6 facilitates the production of IL-21 by T cells which aids B cell affinity maturation and antibody production.(Liu et al., 2013; Nurieva et al., 2009; Nurieva and Chung, 2010) T_{FH} cells also

secrete cytokines that align with their subset classifications (but are not limited to them), such as IFN□ ($T_{FH}1$), IL-4/IL-13 ($T_{FH}2$), IL-4/IL-5/IL-13 ($T_{FH}13$), and IL-17 ($T_{FH}17$) that direct antibody isotype class switching and mediate effector functions.(Bélanger and Crotty, 2016; Crotty, 2014; Gong et al., 2019; Gowthaman et al., 2019; Olatunde et al., 2021; Seth and Craft, 2019)

Several studies have characterized cT_{FH} subsets within the context of both adult and childhood *Pf*-malaria infections, as well as in healthy malaria-naïve volunteers under controlled malaria infection conditions.(Chan et al., 2020) In Mali, where malaria is seasonal, Obeng-Adjei and colleagues showed that T_H1-polarized cT_{FH} $PD1^{pos}CXCR5^{pos}CXCR3^{pos}$ were preferentially activated in children, and were less efficient than the $CXCR3^{neg}$ cT_{FH} in helping autologous B-cells produce antibodies; yet they used U.S. healthy adult cT_{FH} cells for their *in vitro* assays. Therefore, the authors suggested that promoting Th2-like $CXCR3^{neg}$ cT_{FH} subsets could improve antimalarial vaccine efficacy.(Obeng-Adjei et al., 2015) Similarly, a recent study in Papua, Indonesia where malaria is perennial, found that all cT_{FH} subsets from adults showed higher activation and proliferation compared to cT_{FH} cells from children.(Oyong et al., 2022) After *in vitro* stimulation with infected red blood cells, they found that all cT_{FH} subsets were activated in adults accompanied by IL-4 production, whereas only the T_H1-polarized cT_{FH} subset responded in children.(Oyong et al., 2022) One study in Uganda where malaria is holoendemic with seasonal peaks, was able to show that a shift from T_H2- to T_H1-polarized cT_{FH} subsets occurred during the first 6 years of life, and was associated with the development of functional antibodies against *Pf*-malaria; yet appeared to be independent of malaria exposure as this age-associated shift was also observed in a malaria naïve population.(Chan et al., 2022) Interestingly, this study also found that a higher proportion of T_H17-cT_{FH} cells was associated with a decreased risk of *P. falciparum* infection the following year, however the authors postulated that this phenomenon could have been

driven by previous exposure to the parasite. The observed higher abundance of T_H2-like cT_{FH} cells in children younger than 6 years old and the age-associated increase in T_H1-cT_{FH} cells achieving the same proportion of T_H1-cT_{FH} cells by 6 years of age and into adulthood appeared to be independent of malaria exposure. Of note, these studies were limited by the use of a 2-dimensional gating strategy to classify cT_{FH} subsets and whole parasite activation conditions, either during infections or *in vitro* stimulation assays, leaving the malaria-antigen specificity of the different cT_{FH} subsets responses undefined. However, these studies highlight the progression in the field of evaluating the role of human T_{FH} cells in anti-malarial immunity.

Antibody levels are an unreliable predictor of malaria vaccine efficacy.(Stanisic and McCall, 2021) Thus, establishing a combined immune profile to incorporate other surrogates of protection is warranted. Here, we examined the profile of cT_{FH} subsets using multiparameter spectral flow cytometry(Bentebibel et al., 2015; Wei et al., 2015) against two malaria vaccine candidate antigens (*Pf*SEA-1A(Raj et al., 2014) and *Pf*GARP(Raj et al., 2020)) in a cross-section of children and adults residing in a malaria holoendemic region of Kenya. Our findings revealed significant differences in cT_{FH} subsets between children and adults, where children had more abundant $cT_{FH}1$-like cells and showed antigen-specific responses from all cT_{FH} types whereas these responses were limited to $cT_{FH}17$- and 1/17-like in adults. Moreover, this study showed that *Pf*GARP triggered Bcl6 expression across cT_{FH} subsets whereas *Pf*SEA-1A induced more cMAF expression, demonstrating the feasibility of implementing T cell immune correlates to down-select new malaria candidates.

Results

Children had lower anti-PfSEA-1A antibodies compared to adults but similar levels of anti-PfGARP antibodies

This cross-sectional study selected a convenience sample of 7 years old children and adults with a mean age of 22.67 years (ranging from 19 to 30 years old). No statistical difference was observed (p=0.35 after Welch's test) regarding the absolute lymphocyte count (ALC) between children (mean of 373.1; SD of 118.1) and adults (mean of 335.2; SD of 99.08). Children had significantly lower hematocrit (median of 37%, IQR of 32.7-40.5) compared to adults (median of 44.4%, IQR of 40.5-46), p=0.002 after a two-tailed Mann-Whitney t-test, however these values are within normal ranges adjusting for age.(Pluncevic Gligoroska et al., 2019) Both males and females (sex assigned at birth) were enrolled, with 43% (6/14) and 54% (8/15) being female within the children and adult groups, respectively. Seroprofiles against a panel of commonly used malaria antigens were generated to confirm the history of previous malaria infections for the selected children (Figure 1a). All participants had high IgG levels against AMA-1 and MSP1 (merozoite antigens), confirming at least one malaria infection within their lifetime.(O'Flaherty et al., 2021; Yman et al., 2019) IgG antibodies against CSP and CelTOS (liver-stage antigens) were characteristically lower than against blood-stage antigens yet were present in all study children. We observed a clear bimodal distribution in antibody levels against HRP2 with half of the children having "high-HRP2" versus "low-HRP2" IgG levels, possibly a reflection of recent malaria history, since it has been suggested that HRP2-specific antibodies are short-lived and could serve as a surrogate for a recent infection.(Turnbull et al., 2022) Serological profiles were then assessed for two *Pf*-malaria antigens being considered as potential vaccine candidates,(Raj et al., 2020, 2014) *Pf*SEA-1A and *Pf*GARP (Figure 1b). We found that children had a significantly lower median level of IgG against *Pf*SEA-1A compared to adults (p<0.0001), whereas median levels to *Pf*GARP were similarly high for adults and children, yet with a broad range of reactivity.

The overall abundance of the CD4^{pos}CXCR5^{pos} cells is unaltered by in vitro antigen stimulation

To determine whether *in vitro* antigen stimulation with *Pf*SEA-1A or *Pf*GARP altered the abundance of total cT$_{FH}$ cells, we compared cT$_{FH}$ cells from adults and children using a FlowSOM unbiased clustering analysis and EMBEDSOM dimensional reduction based on common lineage markers assessed by spectral flow cytometry from 87,812 lived lymphocytes from each sample: CD8^{pos}, CD4^{pos}, CD4^{pos}CXCR5^{pos}, and CD4^{pos}CD25^{pos} (Figure 2a). As expected after a short stimulation (6 hrs), their overall abundances were similar across conditions for both adults (Figure 2b), and children (Figure 2c). This observation was confirmed by EdgeR statistical analysis (Supplemental Figure 2) and demonstrated that *in vitro* stimulation did not preferentially expand the T cell populations on which we based our subsequent analyses.

An unbiased clustering analysis identifies twelve distinct cT$_{FH}$ meta-clusters

Numerous markers and a two-dimensional gating strategy have previously been used to determine the frequency of cT$_{FH}$ subsets.(Chan et al., 2022; Obeng-Adjei et al., 2015; Oyong et al., 2022) To simultaneously account for the expression of 17 markers required to define cT$_{FH}$ subsets, we used FlowSOM unbiased clustering analysis to determine the frequency of cT$_{FH}$ subsets from a pool of 1,000 CD3^{pos}CD4^{pos}CXCR5^{pos}CD25^{neg} cells from each sample (total of 13,000 CD3^{pos}CD4^{pos}CXCR5^{pos}CD25^{neg} cells in both children and adult). Based on CXCR3 and CCR6 expression as well as the expression of effector/memory/activation markers (CCR7, CD127, PD1, ICOS), cytokines (IFN□, IL-4, and IL-21) and transcription factors (Bcl6, cMAF), we initially identified 15 meta-clusters within the CD4^{pos}CXCR5^{pos} T cells (Figure 3a). First, we found different CXCR5 expression levels between meta-clusters (Figure 3b), suggesting different capabilities of cT$_{FH}$ to migrate to the lymph nodes and,

therefore, to interact with B-cells, i.e., cT_{FH} cells with lower CXCR5 expression would be less likely to reach the B-cell zone. Data presented in Figure 3 are from children, however, similar observations were made for adults (Supplemental Figure 3). Because $CD45RA^{pos}CXCR5^{pos}$ cells are likely naive cells with transient low expression of CXCR5 yet expressing high CD45RA, we excluded 3 meta-clusters using these criteria (i.e., MC12, MC14, and MC15) (Figure 3c). Then, using the overall expression of CXCR3 and CCR6 across the cT_{FH} subsets (Figure 3d and 3e), we identified the remaining 12 clusters as follows: MC01 and MC02 were $cT_{FH}2$-like; MC06 and MC07 were $cT_{FH}1$-like; MC09 and MC11 were $cT_{FH}1/17$-like; MC10 and MC13 were $cT_{FH}17$-like;. However, CXCR3 expression was not clearly delineated for some subsets and did not align with the conventional CCR6 vs CXCR3 cytoplot (Figure 3f and 3g, supplemental figure 4). Based on the heatmap (Figure 3f), MC03, MC04, MC05 and MC08 clusters appear closer to $cT_{FH}2$-like MC01 and MC02 than $cT_{FH}1$-like clusters MC06 and MC07 suggesting that they might be part of the $cT_{FH}2$-like subset. But, based on their intensity of CXCR3 expression and their distribution across the CCR6 vs CXCR3 cytoplot (supplemental figure 4) we defined MC03, MC04, MC05, MC08 as "undetermined" and would require additional cytokine and transcription factor characterization to fully categorize them.

Heterogeneity of activation/maturation markers within cT_{FH} subsets

By assessing the expression of CCR7, PD1, CD127, and ICOS (Figure 4) and following the three-dimensional expression patterns adapted from Schmitt et. al(Schmitt et al., 2014) (Supplemental Figure 5), we determined the activation state of each cT_{FH} meta-cluster and which markers created novel subsets. Data represented in Figure 4 are from children; however, similar observations were made for adults (Supplemental Figure 6). As expected, none of the extracellular markers showed significant differences in expression patterns after a

short 6 hrs stimulation, thus representing the cT_{FH} repertoire present within our study participants. Interestingly, the cT_{FH}1or2 subset (MC03) was the only meta-cluster with high expression of PD1 (Figure 4a) and accompanied by high ICOS (Figure 4b), low CCR7 (Figure 4c), and low expression of CD127 (Figure 4d) suggesting that MC03 was an activated/effector cT_{FH}1or2 subset. Low CCR7 and high ICOS but with low CD127 and PD1 expression indicated that MC04 was a less activated/effector cT_{FH}1or2 subset compared to MC03. Additional nuances in expression pattern were also observed for other cT_{FH}1-like meta-clusters: cT_{FH}1-like MC06 had an activated/effector profile whereas cT_{FH}1-like MC07 had a quiescent/effector profile; cT_{FH}1or2-like MC05 and MC08 were defined as quiescent/memory (overall high CCR7 expression) yet with very low expression of ICOS for MC05. Likewise, cT_{FH}2-like and cT_{FH}17-like meta-clusters also displayed heterogeneity: cT_{FH}2-like MC01 had an activated/effector profile whereas cT_{FH}2-like MC02 seemed to be a quiescent/effector subset; cT_{FH}1/17-like subsets MC09 and MC11 overall had an activated profile even though they had higher expression of CCR7 and CD127 compared to other subsets, suggesting an activated/memory phenotype; and finally cT_{FH}17-like MC10 seemed quiescent whereas cT_{FH}17-like MC13 had an activated/effector profile. Of note, because of our short stimulation time (6H) we were not able to assess CD40L expression (supplemental figure 7). However, our analysis methods revealed a higher degree of previously unrecognized heterogeneity within circulating cT_{FH} cells.

Activated cT_{FH}1or2-, cT_{FH}1-, and quiescent cT_{FH}1or2-like subsets were more abundant in children

After having deconvoluted cT_{FH} cells into 12 subsets, we next wanted to determine whether their abundance differed by age or after antigen stimulation. Using UMAP visualization, we found that cT_{FH} dimensional reduction was contiguous as meta-clusters merged with each

other; in addition, there were notable differences between adults and children (Figure 5a). We found that activated PD1^{high} cT$_{FH}$1or2-like (MC03), activated cT$_{FH}$1-like (MC06), and quiescent ICOS^{high} cT$_{FH}$1or2-like (MC08) subsets were significantly more abundant in children compared to adults regardless of the stimulation conditions (Figure 5b, 5c and 5d, $p<0.05$). In contrast, quiescent cT$_{FH}$2-like cells (MC02) were significantly more abundant in adults compared to children after both *Pf*SEA-1A and *Pf*GARP stimulations (Figure 5c and 5d, $p<0.05$). Interestingly, following *Pf*GARP stimulation, the activated cT$_{FH}$1/17-like subset MC09 became more abundant in children compared to adults (Figure 5d, $p<0.05$ with FDR=0.08); but no additional subsets expanded after *Pf*SEA-1A stimulation (Figure 5c). Of note, activated PD1^{low} cT$_{FH}$1or2-like (MC04) seemed more abundant in non-stimulated adults and *Pf*GARP stimulated children, but, because these observations were not present in all the participants, they did not achieve statistical significance in EdgeR.

The abundance heatmap (Figure 5e) reiterates the differences observed between children and adults and highlights important considerations when assessing the potential role of each cT$_{FH}$ subsets in assisting with cognate antibody production. Overall, the most common cT$_{FH}$ subset in both children and adults is quiescent cT$_{FH}$2-like cells (MC02, 24.1% and 41.2% respectively). However, the antigen-specific differences in cT$_{FH}$ subset abundance for children (MC09 for *Pf*GARP) and for adults (MC02 for both *Pf*SEA-1A and *Pf*GARP) suggest that children engage different cT$_{FH}$ cells as they are developing immunity. Of note, only the activated PD1^{low} cT$_{FH}$1or2-like (MC04) was less abundant in children with low compared to high HRP2 antibody levels (Supplemental Figure 8), suggesting that this subset may be involved in short-term antibody production. Overall, this comprehensive examination of the abundance of cT$_{FH}$ subsets demonstrates important diversity based on age and malaria-antigen specificity.

PfSEA-1A and PfGARP induced IL4, Bcl6 and cMAF from a broad range of cT_{FH} subsets in children

Because the children in this cohort were 7 years of age and resided in a malaria holoendemic area, they had ample time to develop premunition. To assess antigen-specific cytokine and transcription factor expression signatures and further characterize cT_{FH} subsets we generated clustered heatmaps of the MFI of each analyte (IFN□, IL-4, IL-21, Bcl6 and cMAF) for children (Supplemental Figure 9a) and adults (Supplemental Figure 9b). Next, using these MFI data, we performed Wilcoxon paired tests to compare *Pf*SEA-1A and *Pf*GARP stimulation to unstimulated cells (Figure 6a and 6b, respectively). Significant differences in these expression profiles allowed us to further characterize meta-clusters into three main groups. Group 1: cT_{FH}2-like (activated MC01 and quiescent MC02) and activated cT_{FH}1or2-like ($PD1^{high}$MC03 and $PD1^{low}$MC04); Group 2: activated and quiescent cT_{FH}1-like (MC06 and MC07); Group 3: activated cT_{FH}1/17-like (MC11) and cT_{FH}17-like (quiescent MC10 and activated MC13). For children, *Pf*SEA-1A and *Pf*GARP induced robust IL4 expression in 9 out of 12 cT_{FH} meta-clusters (p-values ≤ 0.0105); although the composition of which cT_{FH} subsets were engaged differed slightly by antigen (quiescent cT_{FH}1or2-like $ICOS^{low}$ MC05 versus quiescent cT_{FH}2-like MC02, respectively). In contrast to IL-4, we observed no change in expression for IFN□ or IL-21 after *in vitro* antigen stimulation (except for quiescent cT_{FH}1or2-like $ICOS^{high}$ MC08, p-value = 0.0391), suggesting these cytokines are not informative to define the development of antigen-specific cT_{FH} subsets in children.

We found that *Pf*SEA-1A (Figure 6a) and *Pf*GARP (Figure 6b) induced similar Bcl6 and cMAF expression profiles from some of the same cT_{FH} subsets: both transcription factors were expressed by activated cT_{FH}2-like MC01 and quiescent cT_{FH}17-like MC10, but only cMAF was expressed in activated and quiescent cT_{FH}1-like MC06, MC07 and activated cT_{FH}1/17-like MC11. However, *Pf*SEA-1A induced Bcl6 and cMAF from activated

PD1^{high}MC03 whereas *Pf*GARP only induced Bcl6. In contrast, quiescent cT_{FH}2-like MC02 did not seem to respond to *Pf*SEA-1A (only cMAF was significant, *p*=0.0266, Figure 6a, Supplemental Figures 10 and 11), whereas *Pf*GARP stimulation induced significantly more IL-4, Bcl6, and cMAF compared to unstimulated cells (*p*=0.0081, *p*=0.0017, and *p*=0.0081, respectively, Figure 6b, Supplemental Figures 10 and 11). We then compared the response intensity between *Pf*SEA-1A and *Pf*GARP stimulations, and found significant differences in IFN□, IL21, Bcl6, and cMAF expression levels (Figure 6c, 6d, 6e and 6f, respectively). In Group 1, Bcl6 expression was significantly higher within activated and quiescent cT_{FH}2-like (MC01 and MC02) as well as activated PD1^{high} cT_{FH}1or2-like (MC03) meta-clusters after *Pf*GARP compared to *Pf*SEA-1A stimulation (*p*=0.0266, *p*=0.0134 and *p*=0.0327, respectively, Figure 6e). Within Group 2, IFN□ and Bcl6 were found to be highly expressed by activated cT_{FH}1-like (MC06) after *Pf*GARP compared to *Pf*SEA-1A stimulation (*p*=0.0093 and *p*=0.0024, respectively, Figure 6c and 6e). Finally, within Group 3, activated cT_{FH}1/17-like (MC11) expressed higher cMAF after *Pf*SEA-1A stimulation compared to *Pf*GARP (p=0.0186, Figure 6f). Interestingly, *Pf*GARP induced significantly more IL21 within the quiescent ICOS^{low} cT_{FH}1or2-like (MC05) meta-cluster compared to *Pf*SEA-1A stimulation (*p*=0.0186, Figure 6d). Non-significant differences in cytokines and transcription factors expressed by cT_{FH} subsets between conditions are shown in Supplemental Figures 12 and 13, respectively.

PfGARP induced IL4, Bcl6 and cMAF expression in activated cT_{FH}1/17- and cT_{FH}17-like subsets in adults

A similar heatmap was generated for adult expression profiles comparing *Pf*SEA-1A and *Pf*GARP stimulation to unstimulated cells (Figure 7). Here, we found that both *Pf*SEA-1A and *Pf*GARP induced significant expression of both IFN□ and IL-4 for activated (MC01) and

quiescent (MC02) $cT_{FH}2$-like cells (Figure 7a and 7b, Supplemental Figure 12). Whereas, *Pf*GARP also induced IL-4 and IFN□ expression from quiescent and activated $cT_{FH}17$-like (MC10 and MC13), in addition to Bcl6 and cMAF for MC13 (Figure 7b, Supplemental Figure 13). This observation was surprising because IFN□-expression is commonly used to categorize the $cT_{FH}1$ subset (Group 2); however, as shown earlier, quiescent and activated $cT_{FH}17$-like (MC10 and MC13) did not express CXCR3 (Figure 3d and 3e). In contrast, activated $cT_{FH}1/17$-like (MC11) only responded to *Pf*GARP (Figure 7b, Supplemental Figure 12), expressing higher levels of IL-4, IL-21, Bcl6, and cMAF. Finally, while assessing the differences between the two malaria antigens, we found that *Pf*GARP induced more Bcl6 expression than *Pf*SEA-1A within quiescent $cT_{FH}2$-like (MC02, p=0.0327) and quiescent $ICOS^{low}$ $cT_{FH}1or2$-like (MC05, p=0.0105), as well as within quiescent $cT_{FH}17$-like (MC10 p=0.0479) and activated $cT_{FH}1/17$-like (MC11 p=0.0020) (Figure 7d), the latest expressing higher IL21 as well after *Pf*GARP compared to *Pf*SEA-1A stimulation (p=0.0273, Figure 7c); whereas *Pf*SEA-1A induced cMAF within activated $cT_{FH}2$-like (MC01, p=0.0134) but *Pf*-GARP did not (Figure 7e). Overall, the main observation for adults is that *Pf*SEA-1A predominantly induced IL-4 from slightly more than half of the cT_{FH} clusters, whereas *Pf*GARP induced a broader range of cytokines and transcription factors but within the activated $cT_{FH}1/17$-like (MC11), quiescent and activated $cT_{FH}17$-like (MC10 and MC13) similar to children. This analysis shows clear differences in cT_{FH} subset specificity by malaria antigen and cT_{FH} subset engagement by age group, with the cT_{FH} repertoire becoming more restricted in adults compared to children.

Activated $cT_{FH}1or2$-like subset is more abundant in participants with high anti-PfGARP antibodies

As shown in Figure 1b, a broad range of anti-*Pf*GARP IgG antibody levels were found within both children and adults. Thus, we wanted to determine whether the abundance of any of the cT_{FH} subsets was associated with the level of anti-*Pf*GARP IgG antibodies. When stratifying by high versus low anti-*Pf*GARP IgG antibody levels, we found that an activated cT_{FH}1or2-like subset (MC04) was more abundant in participants with high levels of anti-*Pf*GARP IgG for both children (Figure 8a) and adults (Figure 8b) after *Pf*GARP stimulation compared to participants with low levels or an absence of anti-*Pf*GARP IgG. However, even though the *p*-values were significant for both children and adults (p=0.02 and p=0.004, respectively), the FDR was less than 0.05 only for the adults (FDR=0.018). This suggests that this particular subset might be important for the generation of anti-*Pf*GARP antibodies. Interestingly, activated cT_{FH}1-like (MC06) and quiescent cT_{FH}1-like (MC07) were more abundant for adults with low or no anti-*Pf*GARP IgG antibodies compared to those with high levels (p=0.0024 with FDR=0.0185 and p=0.0034 with FDR=0.0185, respectively) consistent with previous observations describing T_{FH}1 subsets as not efficient help for antibody production(Obeng-Adjei et al., 2015).

Discussion

The overall aim of this study was to define cT_{FH} subsets using unbiased clustering analysis and assess their malaria antigen-specific (*Pf*SEA-1A and *Pf*GARP)(Duffy and Patrick Gorres, 2020; Raj et al., 2020, 2014) profiles for adults and children residing in a malaria holoendemic area of Kenya. Contrary to previous publications,(Obeng-Adjei et al., 2015; Oyong et al., 2022) our study found that children did not only respond via their cT_{FH}1-like subsets but also engage a broader spectrum of cT_{FH} subsets. In fact, cytokine and transcription factor profiles for children involved cT_{FH}1-, cT_{FH}2-, cT_{FH}17- and cT_{FH}1/17-like subsets (summarized in Figure 9) whereas in adults, the dominant antigen-specific memory

response was from cT_{FH}17- and cT_{FH}1/17-like subsets but only for *Pf*GARP. Thus, revealing a potential difference in engaging cT_{FH} help between the two malaria vaccine candidates evaluated in this study.

Several key points can be made from our results. First, it may be too soon in the field of cT_{FH} biology to select only one or two types of cT_{FH} subset(s) to measure when evaluating malaria vaccine candidates, especially if we miss essential, albeit transient, correlates of protection for children which may differ in adults. Longitudinal studies with clinical outcomes are needed to determine the impact of the changing dynamics of cT_{FH} subset adaptations after repeated malaria infections that lead to premunition and parasite clearance. A Ugandan study by Chan et al(Chan et al., 2022) demonstrated an age-associated change in cT_{FH} subsets independent of malaria and, thus, supports the importance of accounting for age when evaluating antigen-specific cT_{FH} profiles. Second, our study reveals that adults have a robust cT_{FH}17- and cT_{FH}1/17-like subset response to *Pf*GARP but not to *Pf*SEA-1A. In addition to demonstrating differences between malaria antigens, this supports the premise that cT_{FH}17 cells are important for maintaining immunological memory,(Gao et al., 2023) which has intriguing implications for evaluating malaria vaccine efficacy. Third, we found a correlation between cT_{FH}1or2-like (MC04) and high *Pf*GARP antibodies for both children and adults, indicating that a cT_{FH} subset accompanied by high antibody levels could serve as a potential biomarker of protection. More studies are needed to explore this association; however, we postulate that a coalition of cT_{FH} subsets might be engaged to develop long-lived antibody responses and, therefore, categorizing subsets as efficient or inefficient might be context dependent.(Obeng-Adjei et al., 2015)

As the field of computational immunology and unbiased clustering analyses evolves, it presents an ongoing challenge to meaningfully define cT_{FH} subsets. Here, we intentionally chose to use cT_{FH}1or2-like nomenclature for meta-clusters MC03, MC04, MC05, and MC08

(Figure 9) because of their low CXCR3, but not null, and robust IL4 expression (instead of IFNγ along with Bcl6, and cMAF). CXCR3 expression leans towards a $cT_{FH}1$-like polarization, whereas IL4 expression indicates a $cT_{FH}2$-like profile when we follow the most commonly used cT_{FH} classification.(Bentebibel et al., 2015; Olatunde et al., 2021; Schmitt et al., 2014; Seth and Craft, 2019) This difference is crucial as $cT_{FH}2$ cells are described as good promoters for functional GC antibodies(Chan et al., 2020; Oyong et al., 2022) whereas $cT_{FH}1$ cells are not.(Hansen et al., 2017; Obeng-Adjei et al., 2015; Oyong et al., 2022) Therefore, their definitive classification will require a more in depthr investigation. Even though we used malaria antigen-specific stimulation, and not a *Pf*-lysate or infected red blood cells (iRBCs) as previously described,(Chan et al., 2022; Obeng-Adjei et al., 2015; Oyong et al., 2022) adults had significantly more of the quiescent $cT_{FH}2$-like subset (MC02) compared to children who instead had significantly more of the activated $cT_{FH}1$-like subset (MC06), the latest being consistent with previous publications,(Obeng-Adjei et al., 2015; Oyong et al., 2022) and more $PD1^{high}$ activated and $ICOS^{high}$ quiescent $cT_{FH}1or2$-like subsets (MC03 and MC08, respectively). However, even when classifying the cT_{FH} meta-clusters as $cT_{FH}1$, $cT_{FH}2$, $cT_{FH}17$, or $cT_{FH}1/17$; the most abundant cT_{FH} subset was $cT_{FH}2$ cells for adults (more than 50%) contradicting a previous study showing only ~20% of $cT_{FH}2$ cells for the same age range.(Chan et al., 2022) As suggested by Gowthaman's T_{FH} model,(Gowthaman et al., 2019) $T_{FH}1$ cells are involved in the development of neutralization antibody responses to viruses and bacteria whereas parasites, such as helminths, lead to a $T_{FH}2$ response. These observations reinforce the need to assess T_{FH} subset profiles stratified by exposure to potentially immune-modulating co-infections.

Transcription factors cMAF and Bcl6 play essential roles in T_{FH} development and function.(Imbratta et al., 2020; Liu et al., 2012; Nurieva et al., 2009) cMAF induces the expression of various molecules, such as ICOS, PD1, CXCR5, IL4, and IL21, which are all

essential for T_{FH} function.(Imbratta et al., 2020) It was, therefore, not surprising to find that cMAF significantly increased after antigen stimulation for most of the cT_{FH} subsets in children. However, again, this expression profile was only observed in the activated cT_{FH}1/17-like subset (MC11) after *Pf*GARP stimulation in cells from adults, supporting a role for T_{FH}17 cells in the maintenance of immunological memory.(Gao et al., 2023) Importantly, cMAF cooperates with Bcl6 in T_{FH} development and function and is essential to establish an efficient GC response.(Nurieva et al., 2009; Yu et al., 2009) Bcl6 is also described as being expressed by mature T_{FH} cells, inducing the expression of CXCR5 and PD1, but it can also regulate IFNγ and IL17 production.(Crotty, 2014; Johnston et al., 2009; Nurieva et al., 2009; Yu et al., 2009) In our study, *Pf*GARP induced a highly significant increase of Bcl6 in cT_{FH}2-like and cT_{FH}17-like subsets in children, suggesting that *Pf*-GARP may be a better candidate to trigger an efficient humoral response in children compared to *Pf*SEA-1A. Of note, Blimp1, a Bcl6 antagonist,(Johnston et al., 2009) was absent from our flow panel and would be of interest to assess in future studies.

There are several limitations of human immune profiling studies. Similar to other such studies, we used peripheral blood and, thus, were only able to provide a snapshot of the cT_{FH} cells. Study participants did not have blood stage malaria infections at the time of blood collection and children were 7 years of age; thus, our profiles were by design meant to reflect cT_{FH} memory recall responses and demonstrate differences between children and adults. As this was not a birth cohort study design, it is possible that the number of cumulative malaria infections could have confounded the association between malaria and cT_{FH} subsets causing a certain cT_{FH} meta-cluster to arise. Most human immunology studies are unable to assess tissue-resident T_{FH} or T_{FH} in the lymph nodes, and, therefore, we are only able to speculate on the composition of T_{FH} cells observed in children that were perhaps short-lived helper and not maintained as T cell memory, or alternatively may have trafficked from the blood into

tissues over time.(Potter et al., 2021) Using an *in vivo* non-human primate model, Potter et al., showed an entry rate of lymphocyte subsets into peripheral lymph nodes per hour of 1.54% and 2.17% for $CD4^{pos}$ central memory ($CD45^{neg}CCR7^{pos}$) and effector memory ($CD45^{neg}CCR7^{neg}$) T cells, respectively,(Potter et al., 2021) both of which may include central and effector memory cT_{FH} cells. With this in mind, cT_{FH} cells seem to be at a crossroad with multiple possible fates. The first one being the recirculation of cT_{FH} cells from lymph node to lymph node whereby a peripheral blood sampling captures migratory cT_{FH} subsets, which could explain the cT_{FH} subsets we observed still expressing cMAF and Bcl6. A decade ago, it was hypothesized that once a T_{FH} cell leaves the lymph node, it can become a $PD1^{low}$ memory cT_{FH} cell with the possibility of returning to a germinal center T_{FH} stage after a secondary recall response.(Crotty, 2014) Other possible fates include becoming a $PD1^{neg}$ memory cT_{FH} with the same path after recall or progressing to a non-T_{FH} cell.(Crotty, 2014) More recently, a few studies showed circulating $CXCR5^{neg}CD4^{pos}$ cells with T_{FH} functions, such as production of IL21 and the capability to help B cells in systemic lupus erythematosus and HIV-infected individuals,(Bocharnikov et al., 2019; Del Alcazar et al., 2019) and importantly they mapped these circulating $CXCR5^{neg}CD4^{pos}$ cells to an original lymph node $CXCR5^{pos}$ T_{FH} subset,(Del Alcazar et al., 2019) suggesting another possible outcome for T_{FH} cells outside secondary lymphoid organs. To date, no clear destiny has been established for cT_{FH} cells in humans, thus, highlighting the importance of including a complete panel of cT_{FH} subsets to continue to improve our understanding of their respective roles against different pathogens and eliciting long-lived vaccine-induced antibody responses.

Other limitations of this study include not measuring other cytokines (i.e., IL5, IL13, IL17) and transcription factors (i.e., T-bet, BATF, GATA3, RORγt) that have been used in other studies to fully characterize cT_{FH} subsets.(Crotty, 2014; Gowthaman et al., 2019) However, even with our small sample size we demonstrated significant age-associated

differences in malaria antigen-specific responses from different cT_{FH} subsets. To minimize false positive results that can arise when using algorithms for computational analyses, we ran the statistical tests in triplicate and the clustering algorithm in duplicate, to validate our findings.

In summary, our study provides additional justification for the resources needed to conduct cellular immunological studies that include cT_{FH} cell signatures and provides insight into which types of cT_{FH} subset during a person's lifespan assist germinal center B cells to produce long-lived plasmocytes and functional antibodies(Moormann et al., 2019) against malaria. This is particularly important when selecting immune correlates of protection that could be used to predict the efficacy of the next generation of *Pf*-malaria vaccine candidates within various study populations.

Methods

Study populations and ethical approvals

Adults and children were recruited from Kisumu County, Kenya which is holoendemic for *Pf*-malaria. Written informed consent was obtained from each adult participant and children guardian. An abbreviated medical history, physical examination, and blood film were used to ascertain health and malaria infection status at the time of blood sample collection. Participants were also life-long residents of the study area with an assumption that they naturally acquired immunity to malaria. This study was conducted prior to the implementation of any malaria vaccines. Participants were eligible if they were healthy and not experiencing any symptoms of malaria at the time venous blood was collected. For this cross-sectional immunology study, we selected fourteen 7-years old children from a larger age-structured prospective cohort study (enrollment age range 3-7 years) and fifteen Kenyan adults. We selected 7-year olds because of the age-dependent shift in major cT_{FH} subsets

occurring after 6-years of age(Chan et al., 2022), and as a comparable age published by other studies(Obeng-Adjei et al., 2015), in order to maximize our ability to measure antigen-specific differences in T_{FH} subsets.

Ethical approvals were obtained from the Scientific and Ethics Review Unit (SERU) at the Kenya Medical Research Institute (KEMRI) reference number 3542, and the Institutional Review Board at the University of Massachusetts Chan Medical School, Worcester, MA, USA, IRB number H00014522. Brown University, Providence, RI, USA signed a reliance agreement with KEMRI.

Plasma and PBMCs isolation

Venous blood was collected in sodium heparin BD Vacutainers and processed within 2 hours at the Center for Global Health Research, KEMRI, Kisumu. Absolute lymphocyte counts (ALC) were determined from whole blood using BC-3000 Plus Auto Hematology Analyzer, 19 parameters (Shenzhen Mindray Bio-Medical Electronics Co.). After 10 mins at 1,000g spin, plasma was removed and placed for storage at -20°C and an equivalent volume of 1X PBS was added to the cell pellet. Peripheral blood mononuclear cells (PBMCs) were then isolated using Ficoll-Hypaque density gradient centrifugation on SepMate (StemCell). PBMCs were frozen at $5x10^{6}$ cells/ml in a freezing medium (90% heat-inactivated and filter-sterilized fetal bovine serum (FBS) and 10% dimethyl sulfoxide (Sigma)) and chilled overnight in Mr. Frosty™ containers at -80°C prior being transferred to liquid nitrogen. Transport to the USA used an MVE vapor shipper (MVE Biological Solutions) to maintain the cold chain.

In-vitro stimulation assay

PBMCs were thawed in 37°C filtered-complete media (10% FBS, 2mM L-Glutamine, 10mM HEPES, 1X Penicillin/Streptomycin) and spun twice before resting overnight in a 37°C, 5% CO_2 incubator. PBMCs were counted using Trypan Blue (0.4%) and hemocytometer, and the

cell survival was calculated. Our samples showed a median of 94.6% live cells [25% percentile of 92%; 75% percentile of 97%]. Using a P96 U-bottom plate, $1x10^6$ PBMCs per well were placed in culture with one of the following stimulation conditions: *Pf*SEA-1A(Raj et al., 2014) (5 µg/ml) or *Pf*GARP(Raj et al., 2020) (10 µg/ml) both produced in the Kurtis lab (Brown University); SEB (1 µg/ml; EMD Millipore) as a positive control; sterile water (10µl, the same volume used to reconstitute *Pf*SEA and *Pf*GARP) as a negative control. A pool of anti-CD28/anti-CD49d (BD Fast-Immune Co-Stim following the manufacturer's instructions), GolgiSTOP (0.7 µg/ml), and GolgiPLUG (0.1 µg/ml) (BD Biosciences) were added to each well before incubating cells at 37^oC for 6-hours.

Cell staining and Flow cytometry

A multiparameter spectral flow cytometry panel was used to characterize cT_{FH} cell subsets: CCR6-BV421 (RRID: AB_2561356), CD14-Pacific Blue (RRID: AB_830689), CD19-Pacific Blue (RRID: AB_2073118), CCR7-BV480 (RRID: AB_2739502), IFNγ-BV510 (RRID: AB_2563883), CD127-BV570 (RRID: AB_10900064), CD45RA-BV605 (RRID: AB_2563814), PD1-BV650 (RRID: AB_2738746), CXCR3-BV711 (RRID: AB_2563533), CD25-BV750 (RRID: AB_2871896), CXCR5-BV785 (RRID: AB_2629528), Bcl6-AF488 (RRID: AB_10716202), CD3-Spark Blue 550 (RRID: AB_2819985), CD8-PerCP-Cy5.5 (RRID: AB_2044010), IL21-PE (RRID: AB_2249025), IL4-PE-Dazzle (RRID: AB_2564036), CD4-PE-Cy5 (RRID: AB_314078), ICOS-PE-Cy7 (RRID: AB_10643411), cMAF-eFluor 660 (RRID: AB_2574388), CD40L-AF700 (RRID: AB_2750053), and Zombie NIR (BioLegend cat# 423106) for Live/Dead staining. Data was acquired on a Cytek Aurora with 4-lasers (UMass Chan Flow Core Facility) using SpectroFlo® software (Cytek) and compensation for unmixing and fluorescence-minus-one controls. Quality control of the data was performed using SpectroFlo®, and the multi-parameter analysis was performed with OMIQ data analysis software (www.omiq.ai). Thus, we assessed the expression of markers

commonly used to define the following different cT_{FH} ($CD4^{pos}CD25^{neg}CXCR5^{pos}$) subsets: $cT_{FH}1$-like ($CCR6^{neg}CXCR3^{pos}$), $cT_{FH}2$-like ($CCR6^{neg}CXCR3^{neg}$), and $cT_{FH}17$-like ($CCR6^{pos}CXCR3^{neg}$),(Schmitt et al., 2014) as well as quiescent/central memory cT_{FH} ($CCR7^{high}PD\text{-}1^{neg}ICOS^{neg}$) or activated/effector memory cT_{FH} cells ($CCR7^{low}PD\text{-}1^{pos}ICOS^{pos}$).(Gong et al., 2019; Schmitt et al., 2014) Representative cytoplots can be found in supplemental figure 1.

Multiplex suspension bead-based serology assay

To measure plasma IgG antibody levels to *Pf*SEA-1A(Raj et al., 2014) and *Pf*GARP(Raj et al., 2020), we used a Luminex bead-based suspension assay as previously published.(Cham et al., 2009; Forconi et al., 2018) In addition, previous *Pf* exposure was determined using recombinant proteins to blood-stage malaria antigens: apical membrane antigen 1 (AMA1) and merozoite surface protein (MSP1), HRP2, CelTos, CSP (gifts from Sheetji Dutta, Evelina Angov, and Elke Bergmann from the Walter Reed Army Institute of Research). Briefly, 100µg of each antigen or BSA (Sigma), as a background control, were coupled to ~$12x10^6$ non-magnetic microspheres (BioRad carboxylated beads) and then incubated with study participant plasma (spun down 10,000g for 10 mins and diluted at 1:100 in the assay dilution buffer) for 2 hrs, followed by incubation with biotinylated anti-human IgG (BD #555785) diluted 1:1000 for 1hr and streptavidin (BD #554061) diluted 1:1000 for 1 hr following the manufacturer's instructions. The mean fluorescence intensity (MFI) of each conjugated bead (minimum of 50 beads per antigen) was quantified on a FlexMap3D Luminex multianalyte analyzer (Xponent software). Results are reported as antigen-specific MFI after subtracting the BSA value for each individual, since background levels can vary between individuals.

OMIQ analysis

The fcs files were uploaded into the OMIQ platform after passing QC under SpectroFlo® (Cytek) where compensation was re-checked. In OMIQ, we arcsinh-transformed the scale to

allow downstream analysis and then gated on singlet live lymphocytes and sub-sampled the data to yield 87,712 live lymphocytes per sample. Using only lineage markers CD3, CD4, CD8, CD14, CD19, CXCR5 and CD25, FlowSOM consensus meta-clustering was run on 100 clusters based on the 87,712 live lymphocytes per sample with a comma-separated k-value of 75, and Euclidean distance metric. Using these 75 meta-clusters, we defined subsets of cells based on lineage markers, such as $CD3^{pos}CD8^{pos}$, $CD3^{neg}CD14^{pos}CD19^{pos}$, and $CD3^{pos}CD4^{pos}$, and then distinguished $CD4^{pos}CXCR5^{pos}CD25^{neg}$ (cT_{FH}) and $CD4^{pos}CXCR5^{neg}CD25^{pos}$ (T regulatory [T_{reg}] or T follicular regulatory [T_{FR}]) subsets. CD25 was used to exclude T_{reg} and T_{FR} cells which share numerous markers with cT_{FH} cells.(Sage et al., 2014; Wing et al., 2018; Zhao et al., 2020) EmbedSOM dimensional reduction was used to visualize the different groups of cells and EdgeR analysis was run to assess the significance of their differences. A clustering heatmap was used to visualize cytokine expression and transcription factor profiles for each subset.

Focusing on the $CD4^{pos}CXCR5^{pos}CD25^{neg}$ T_{FH} cells, we ran another FlowSOM analysis based on the 1,000 $CXCR5^{pos}$ cells per sample (two samples from the adult's group and one sample from the children group were excluded from the analysis as they had less than 1,000 $CXCR5^{pos}$ cells), using extracellular markers CXCR5, CXCR3, CCR6, ICOS, CCR7, CD45RA, CD127, CD40L and PD1 allowing the identification of 15 meta-clusters. From there, we performed Uniform Manifold Approximation and Projection (UMAP) dimensional reduction, heatmaps, and EdgeR analyses, the latter allowing statistical analysis of the cT_{FH} abundances. To demonstrate the reproducibility of these results, statistical analysis algorithms were run at least three times downstream of the same clustering algorithm and downstream of repeated clustering algorithms. To assess statistical differences in cytokines and transcription factor expression, we exported the statistics dataset from OMIQ containing MFI values from each marker (IFN□, IL-4, IL-21, Bcl6 and cMAF) per cluster

and for each sample and stimulation condition. To assess cytokines and transcription factors without bias, we chose to use the total MFI expression per meta-cluster with the assumption that cells with an increased production of the desire analyte will trigger an increase of the overall meta-cluster MFI compared to unstimulated cells, and if there is no production of the desire analyte, the overall MFI will not differ.

Statistical analysis

For this cross-sectional immunology study, we selected both male and female, sex defined at birth, fourteen 7-year-old children and fifteen adults. Using GraphPad Prism software (version 7.0), age, sex, absolute lymphocyte count (ALC), and serological data were compared between adults and children. Because the number of participants within each group was too low to verify the normality of the underlying distributions (adults n=15 and children n=14), we chose to use non-parametric tests, including the Mann-Whitney U test (for unpaired analysis) and Wilcoxon signed-rank test (for paired analysis). When data passed the Normality test (D'Agostino and Pearson test), we used Welch's parametric test. All tests were two-tailed with a *p-value* < 0.05 for significance. Because of the exploratory nature of the analysis, we did not use any adjustment of the *p*-value for multiple comparisons. The tests used are indicated in the legend of each figure. Results were expressed using the mean with standard deviation for dot plots, and exact *p*-values.

To perform a statistical analysis of the cytokine and transcription factor expression from each cT_{FH} subset, the exported data file from OMIQ was integrated into GraphPad Prism, and a non-parametric Wilcoxon paired-*t*-test, two-tailed, analysis was done (n=13 in each group). As this analysis generated numerous bar plots (all included in the supplemental figures 12 to 15), in order to have a better visualization of the cytokines and transcription factors patterns, the *p*-values obtained from each analysis are presented using a non-clustering heatmap.

Role of the funding source

Funders had no role in the study design; the collection of the samples, the analysis and the interpretation of the data as well as the writing of the manuscript and its decision to be submitted for publication.

Contributors

CN, JMO, JK and AMM designed research study; CF and SPT conducted experiments; CF, JK and AMM analyzed data; CF, SPT, JK and AMM contributed to experimental design; HWW, BO, JMO, JK and AMM conducted and supervised the clinical study and the sampling; CF generated figures; HWW and BO verified underlying data; CF and AMM led manuscript preparation with feedback from all the authors. All authors have read and approved the final version of the manuscript.

Data Availability

Deidentified raw data from this manuscript are available from ImmPort platform under the accession study number SDY2534.

Declaration of Competing Interest

Dr Kurtis was the PI on 1R01AI127699-01A1 which supported this study. He holds several patents related to the use of *Pf*SEA-1 and *Pf*GARP as vaccine candidates for *P. falciparum* and has consulted for and is an equity holder in Ocean Biomedical.

Acknowledgments

The authors would like to thank the children and their families for participating in this study. We thank the field and lab teams for their work collecting data and processing blood samples. We also thank Dr. Melanie Trombly from UMass Chan for proofreading our manuscript. This manuscript was approved for publication by the Kenya Medical Research Institute.

This study was supported by NIH R01 AI127699 (Kurtis).

References

Amanna IJ, Carlson NE, Slifka MK. 2007. Duration of humoral immunity to common viral and vaccine antigens. *N Engl J Med* **357**:1903–1915.

Andris F, Denanglaire S, Anciaux M, Hercor M, Hussein H, Leo O. 2017. The Transcription Factor c-Maf Promotes the Differentiation of Follicular Helper T Cells. *Front Immunol* **8**:480.

Aydemir O, Janko M, Hathaway NJ, Verity R, Mwandagalirwa MK, Tshefu AK, Tessema SK, Marsh PW, Tran A, Reimonn T, Ghani AC, Ghansah A, Juliano JJ, Greenhouse BR, Emch M, Meshnick SR, Bailey JA. 2018. Drug-Resistance and Population Structure of Plasmodium falciparum Across the Democratic Republic of Congo Using High-Throughput Molecular Inversion Probes. *J Infect Dis* **218**:946–955.

Bélanger S, Crotty S. 2016. Dances with cytokines, featuring TFH cells, IL-21, IL-4 and B cells. *Nat Immunol*.

Bentebibel S-E, Jacquemin C, Schmitt N, Ueno H. 2015. Analysis of human blood memory T follicular helper subsets. *Methods Mol Biol* **1291**:187–197.

Bocharnikov AV, Keegan J, Wacleche VS, Cao Y, Fonseka CY, Wang G, Muise ES, Zhang KX, Arazi A, Keras G, Li ZJ, Qu Y, Gurish MF, Petri M, Buyon JP, Putterman C, Wofsy D, James JA, Guthridge JM, Diamond B, Anolik JH, Mackey MF, Alves SE, Nigrovic PA, Costenbader KH, Brenner MB, Lederer JA, Rao DA, Accelerating Medicines Partnership (AMP) RA/SLE Network. 2019. PD-1hiCXCR5- T peripheral helper cells promote B cell responses in lupus via MAF and IL-21. *JCI Insight* **4**. doi:10.1172/jci.insight.130062

Breitfeld D, Ohl L, Kremmer E, Ellwart J, Sallusto F, Lipp M, Förster R. 2000. Follicular B helper T cells express CXC chemokine receptor 5, localize to B cell follicles, and support immunoglobulin production. *J Exp Med* **192**:1545–1552.

Cham GKK, Turner L, Lusingu J, Vestergaard L, Mmbando BP, Kurtis JD, Jensen ATR, Salanti A, Lavstsen T, Theander TG. 2009. Sequential, ordered acquisition of antibodies to Plasmodium falciparum erythrocyte membrane protein 1 domains. *J Immunol* **183**:3356–3363.

Chan J-A, Loughland JR, de Labastida Rivera F, SheelaNair A, Andrew DW, Dooley NL, Wines BD, Amante FH, Webb L, Hogarth PM, McCarthy JS, Beeson JG, Engwerda CR, Boyle MJ. 2020. Th2-like T Follicular Helper Cells Promote Functional Antibody Production during Plasmodium falciparum Infection. *Cell Rep Med* **1**:100157.

Chan J-A, Loughland JR, de la Parte L, Okano S, Ssewanyana I, Nalubega M, Nankya F,

Musinguzi K, Rek J, Arinaitwe E, Tipping P, Bourke P, Andrew D, Dooley N, SheelaNair A, Wines BD, Hogarth PM, Beeson JG, Greenhouse B, Dorsey G, Kamya M, Hartel G, Minigo G, Feeney M, Jagannathan P, Boyle MJ. 2022. Age-dependent changes in circulating Tfh cells influence development of functional malaria antibodies in children. *Nat Commun* **13**:4159.

Crotty S. 2019. T Follicular Helper Cell Biology: A Decade of Discovery and Diseases. *Immunity* **50**:1132–1148.

Crotty S. 2014. T follicular helper cell differentiation, function, and roles in disease. *Immunity* **41**:529–542.

Crotty S. 2011. Follicular helper CD4 T cells (TFH). *Annu Rev Immunol* **29**:621–663.

Del Alcazar D, Wang Y, He C, Wendel BS, Del Río-Estrada PM, Lin J, Ablanedo-Terrazas Y, Malone MJ, Hernandez SM, Frank I, Naji A, Reyes-Terán G, Jiang N, Su LF. 2019. Mapping the Lineage Relationship between CXCR5+ and CXCR5- CD4+ T Cells in HIV-Infected Human Lymph Nodes. *Cell Rep* **28**:3047–3060.e7.

Duffy PE, Patrick Gorres J. 2020. Malaria vaccines since 2000: progress, priorities, products. *NPJ Vaccines* **5**:48.

Dunham RM, Cervasi B, Brenchley JM, Albrecht H, Weintrob A, Sumpter B, Engram J, Gordon S, Klatt NR, Frank I, Sodora DL, Douek DC, Paiardini M, Silvestri G. 2008. CD127 and CD25 expression defines CD4+ T cell subsets that are differentially depleted during HIV infection. *J Immunol* **180**:5582–5592.

Forconi CS, Cosgrove CP, Saikumar-Lakshmi P, Nixon CE, Foley J, Ong'echa JM, Otieno JA, Alter G, Münz C, Moormann AM. 2018. Poorly cytotoxic terminally differentiated CD56negCD16pos NK cells accumulate in Kenyan children with Burkitt lymphomas. *Blood Adv* **2**:1101–1114.

Gao X, Luo K, Wang D, Wei Y, Yao Y, Deng J, Yang Y, Zeng Q, Dong X, Xiong L, Gong D, Lin L, Pohl K, Liu S, Liu Y, Liu L, Nguyen THO, Allen LF, Kedzierska K, Jin Y, Du M-R, Chen W, Lu L, Shen N, Liu Z, Cockburn IA, Luo W, Yu D. 2023. T follicular helper 17 (Tfh17) cells are superior for immunological memory maintenance. *Elife* **12**. doi:10.7554/eLife.82217

Geneva: World Health Organization. 2022. World malaria report 2022 (No. Licence: CC BY-NC-SA 3.0 IGO). WHO.

Gong F, Zheng T, Zhou P. 2019. T Follicular Helper Cell Subsets and the Associated Cytokine IL-21 in the Pathogenesis and Therapy of Asthma. *Front Immunol* **10**:2918.

Gowthaman U, Chen JS, Zhang B, Flynn WF, Lu Y, Song W, Joseph J, Gertie JA, Xu L, Collet MA, Grassmann JDS, Simoneau T, Chiang D, Berin MC, Craft JE, Weinstein JS, Williams A, Eisenbarth SC. 2019. Identification of a T follicular helper cell subset that drives anaphylactic IgE. *Science* **365**. doi:10.1126/science.aaw6433

Hansen DS, Obeng-Adjei N, Ly A, Ioannidis LJ, Crompton PD. 2017. Emerging concepts in T follicular helper cell responses to malaria. *Int J Parasitol* **47**:105–110.

Holder AA. 1999. Malaria vaccines. *Proc Natl Acad Sci U S A* **96**:1167–1169.

Imbratta C, Hussein H, Andris F, Verdeil G. 2020. c-MAF, a Swiss Army Knife for Tolerance in Lymphocytes. *Front Immunol* **11**:206.

Ippolito MM, Moser KA, Kabuya J-BB, Cunningham C, Juliano JJ. 2021. Antimalarial Drug Resistance and Implications for the WHO Global Technical Strategy. *Curr Epidemiol Rep* **8**:46–62.

Johnston RJ, Poholek AC, DiToro D, Yusuf I, Eto D, Barnett B, Dent AL, Craft J, Crotty S. 2009. Bcl6 and Blimp-1 are reciprocal and antagonistic regulators of T follicular helper cell differentiation. *Science* **325**:1006–1010.

Liu X, Nurieva RI, Dong C. 2013. Transcriptional regulation of follicular T-helper (Tfh) cells. *Immunol Rev* **252**:139–145.

Liu X, Yan X, Zhong B, Nurieva RI, Wang A, Wang X, Martin-Orozco N, Wang Y, Chang SH, Esplugues E, Flavell RA, Tian Q, Dong C. 2012. Bcl6 expression specifies the T follicular helper cell program in vivo. *J Exp Med* **209**:1841–52, S1–24.

Moormann AM, Nixon CE, Forconi CS. 2019. Immune effector mechanisms in malaria: An update focusing on human immunity. *Parasite Immunol* **41**:e12628.

Nixon CE, Park S, Pond-Tor S, Raj D, Lambert LE, Orr-Gonzalez S, Barnafo EK, Rausch KM, Friedman JF, Fried M, Duffy PE, Kurtis JD. 2017. Identification of Protective B-Cell Epitopes within the Novel Malaria Vaccine Candidate Plasmodium falciparum Schizont Egress Antigen 1. *Clin Vaccine Immunol* **24**. doi:10.1128/CVI.00068-17

Nurieva RI, Chung Y. 2010. Understanding the development and function of T follicular helper cells. *Cell Mol Immunol* **7**:190–197.

Nurieva RI, Chung Y, Martinez GJ, Yang XO, Tanaka S, Matskevitch TD, Wang Y-H, Dong C. 2009. Bcl6 mediates the development of T follicular helper cells. *Science* **325**:1001–1005.

Obeng-Adjei N, Portugal S, Tran TM, Yazew TB, Skinner J, Li S, Jain A, Felgner PL, Doumbo OK, Kayentao K, Ongoiba A, Traore B, Crompton PD. 2015. Circulating Th1-Cell-type Tfh Cells that Exhibit Impaired B Cell Help Are Preferentially Activated during Acute Malaria in Children. *Cell Rep* **13**:425–439.

O'Flaherty K, Oo WH, Zaloumis SG, Cutts JC, Aung KZ, Thein MM, Drew DR, Razook Z, Barry AE, Parischa N, Zaw NN, Thu HK, Thi A, Htay WYM, Soe AP, Simpson JA, Beeson JG, Agius PA, Fowkes FJI. 2021. Community-based molecular and serological surveillance of subclinical malaria in Myanmar. *BMC Med* **19**:121.

Olatunde AC, Hale JS, Lamb TJ. 2021. Cytokine-skewed Tfh cells: functional consequences for B cell help. *Trends Immunol* **42**:536–550.

Oyong DA, Loughland JR, Soon MSF, Chan J-A, Andrew D, Wines BD, Hogarth PM, Olver SD, Collinge AD, Varelias A, Beeson JG, Kenangalem E, Price RN, Anstey NM, Minigo G, Boyle MJ. 2022. Adults with Plasmodium falciparum malaria have higher magnitude and quality of circulating T-follicular helper cells compared to children. *EBioMedicine* **75**:103784.

Pluncevic Gligoroska J, Gontarev S, Dejanova B, Todorovska L, Shukova Stojmanova D, Manchevska S. 2019. Red Blood Cell Variables in Children and Adolescents regarding the Age and Sex. *Iran J Public Health* **48**:704–712.

Potter EL, Gideon HP, Tkachev V, Fabozzi G, Chassiakos A, Petrovas C, Darrah PA, Lin PL, Foulds KE, Kean LS, Flynn JL, Roederer M. 2021. Measurement of leukocyte trafficking kinetics in macaques by serial intravascular staining. *Sci Transl Med* **13**. doi:10.1126/scitranslmed.abb4582

Raj DK, Das Mohapatra A, Jnawali A, Zuromski J, Jha A, Cham-Kpu G, Sherman B, Rudlaff RM, Nixon CE, Hilton N, Oleinikov AV, Chesnokov O, Merritt J, Pond-Tor S, Burns L, Jolly G, Ben Mamoun C, Kabyemela E, Muehlenbachs A, Lambert L, Orr-Gonzalez S, Gnädig NF, Fidock DA, Park S, Dvorin JD, Pardi N, Weissman D, Mui BL, Tam YK, Friedman JF, Fried M, Duffy PE, Kurtis JD. 2020. Anti-PfGARP activates programmed cell death of parasites and reduces severe malaria. *Nature* **582**:104–108.

Raj DK, Nixon CP, Nixon CE, Dvorin JD, DiPetrillo CG, Pond-Tor S, Wu H-W, Jolly G, Pischel L, Lu A, Michelow IC, Cheng L, Conteh S, McDonald EA, Absalon S, Holte SE, Friedman JF, Fried M, Duffy PE, Kurtis JD. 2014. Antibodies to PfSEA-1 block parasite egress from RBCs and protect against malaria infection. *Science* **344**:871–877.

RTS,S Clinical Trials Partnership. 2015. Efficacy and safety of RTS,S/AS01 malaria vaccine with or without a booster dose in infants and children in Africa: final results of a phase 3, individually randomised, controlled trial. *Lancet* **386**:31–45.

Sage PT, Alvarez D, Godec J, von Andrian UH, Sharpe AH. 2014. Circulating T follicular

regulatory and helper cells have memory-like properties. *J Clin Invest* **124**:5191–5204.
Schmitt N, Bentebibel S-E, Ueno H. 2014. Phenotype and functions of memory Tfh cells in human blood. *Trends Immunol* **35**:436–442.
Seth A, Craft J. 2019. Spatial and functional heterogeneity of follicular helper T cells in autoimmunity. *Curr Opin Immunol* **61**:1–9.
Stanisic DI, McCall MBB. 2021. Correlates of malaria vaccine efficacy. *Expert Rev Vaccines* **20**:143–161.
Tarlinton D, Good-Jacobson K. 2013. Diversity among memory B cells: origin, consequences, and utility. *Science* **341**:1205–1211.
Taylor SM, Juliano JJ. 2014. Artemisinin combination therapies and malaria parasite drug resistance: the game is afoot. *J Infect Dis*.
Turnbull LB, Ayodo G, Knight V, John CC, McHenry MS, Tran TM. 2022. Evaluation of an ultrasensitive HRP2-based rapid diagnostic test for detection of asymptomatic Plasmodium falciparum parasitaemia among children in western Kenya. *Malar J* **21**:337.
Wei Y, Feng J, Hou Z, Wang XM, Yu D. 2015. Flow cytometric analysis of circulating follicular helper T (Tfh) and follicular regulatory T (Tfr) populations in human blood. *Methods Mol Biol* **1291**:199–207.
Wing JB, Tekgüç M, Sakaguchi S. 2018. Control of Germinal Center Responses by T-Follicular Regulatory Cells. *Front Immunol* **9**:1910.
Yman V, White MT, Asghar M, Sundling C, Sondén K, Draper SJ, Osier FHA, Färnert A. 2019. Antibody responses to merozoite antigens after natural Plasmodium falciparum infection: kinetics and longevity in absence of re-exposure. *BMC Med* **17**:22.
Yu D, Rao S, Tsai LM, Lee SK, He Y, Sutcliffe EL, Srivastava M, Linterman M, Zheng L, Simpson N, Ellyard JI, Parish IA, Ma CS, Li Q-J, Parish CR, Mackay CR, Vinuesa CG. 2009. The transcriptional repressor Bcl-6 directs T follicular helper cell lineage commitment. *Immunity* **31**:457–468.
Zhao X, Jin T, Zheng C, Ma D, Zhang Y. 2020. Imbalance of Circulating Tfh/Tfr Cells in Patients With Parkinson’s Disease. *Front Neurol* **11**:572205.

Figure Legends

Figure 1: *Pf*-malaria IgG sero-profiles for children and adults. (a) IgG antibody levels against AMA1, MSP1, HRP2, CelTos and CSP for children (n=14). The bar plots indicate mean with SD. (**b)** IgG antibody levels against *Pf*SEA-1A and *Pf*GARP comparing children (n=15) and adults (n=15). The bar plots indicate mean with SD. Net MFI values are the antigen-specific MFI values minus the BSA background. Mann-Whitney tests were performed.

Figure 2: Clusters visualization of immune cell types and their abundance. (a) A 100 node and 75-meta-clusters FlowSOM tree was generated on live lymphocytes from all our participants (n=29 children and adults), highlighting $CD3^{pos}CD8^{pos}$, $CD3^{pos}CD4^{pos}$, $CD4^{pos}CXCR5^{pos}$ and $CD4^{pos}CD25^{pos}$ cells. The 5 nodes of the $CD4^{pos}CXCR5^{pos}CD25^{neg}$ population are circled and will be used for the downstream analysis. The colored scale was based on the median arcsinh-transformed marker expression. UMAP plots showing 5 clusters defined as follow: $CD14/CD19^{pos}$ (orange), $CD4^{pos}$ (blue), $CD4^{pos}CXCR5^{pos}$ (red), $CD8^{pos}$ (purple) and $CD4^{pos}CD25^{pos}$ (green) from **(b)** adults (n=15) **(c)** children (n=14) PBMCs after no-stimulation, *Pf*SEA-1A and *Pf*GARP stimulation, respectively from left to right.

Figure 3: Characterization of T_{FH} subsets by CXCR5, CXCR3, CCR6 and CD45RA expression. (a) A new 25 nodes and 15 meta-clusters FlowSOM tree was generated from the 5 $CD4^{pos}CXCR5^{pos}CD25^{neg}$ nodes shown in Figure 2A (CXCR5 expression tree). The colored scale of CXCR5 expression was based on the median arcsinh-transformed with red as the highest and deep blue the absence of CXCR5 expression. **(b)** Box-plots showing CXCR5 expression across all cT_{FH}-like meta-clusters from children (n=13) with no stimulation (blue), and after *in vitro* stimulation with *Pf*GARP (green) or *Pf*SEA-1A (pink). Fifty percent of the data points are within the box limits, the solid line indicates the median, the dash line the mean and the whiskers indicate the range of the remaining data with outliers being outside that range. Similar box-plots are shown for **(c)** CD45RA, **(d)** CXCR3**,** and **(e)** CCR6 expression across all cT_{FH}-like meta-clusters. **(f)** Clustered heatmap showing the median arcsinh-transformed expression for CCR6, CD45RA, CXCR3 and CXCR5 across meta-clusters, red showing the highest expression and blue the lowest. **(g)** Cytoplots of CCR6 vs CXCR3 expression where MC01 is in blue, MC07 in pink, MC11 in yellow and MC13 in green.

Figure 4: cT_{FH} subset activation state determined by PD1, ICOS, CCR7, and CD127. Box-plots showing **(a)** PD1, **(b)** ICOS, **(c)** CCR7, and **(d)** CD127 expression across all cT_{FH}-like meta-clusters from children (n=13) with no stimulation (blue), and after *in vitro* stimulation with *Pf*GARP (green) or *Pf*SEA-1A (pink). Fifty percent of the data points are within the box limits, the solid line indicates the median, the dash line the mean and the whiskers indicate the range of the remaining data with outliers being outside that range.

Figure 5: Differences in abundance of antigen-specific cT_{FH} meta-clusters for adults and children. (a) UMAP plots showing the 12 different cT_{FH} meta-clusters in adults (top three plots, n=13) and in children (bottom three plots, n=13) in the absence of stimulation or after *in vitro* stimulation with *Pf*SEA-1A or *Pf*GARP, from left to right, respectively. Colored circles highlight the meta-clusters showing differences in their abundance between adults and children for each condition. An EdgeR statistical plot was performed to assess the change in abundance of the 12 meta-clusters between adults and children after **(b)** no stimulation, **(c)** *Pf*SEA-1A and **(d)** *Pf*GARP stimulations. EdgeR plots indicate which meta-clusters are significantly abundant between two groups by using green color dots. The Y-axis is the -log10(*p*-value) and the X-axis is the log(FC). Green dots were statistically significant ($p<0.05$). Numbers next to the dots indicate the meta-cluster. **(e)** An abundance heatmap indicates the percentage (black numbers) of each meta-cluster within the total number of $CD3^{pos}CD4^{pos}CXCR5^{pos}CD25^{neg}$ cells for adults and children (concatenated from 13 participants in each group) under the different conditions: no stimulation (Neg) or stimulation with *Pf*SEA-1A or *Pf*GARP. The color scale ranges from high expression (red) to low/no expression (blue). The star in the heatmap indicates which meta-cluster is significantly abundant in children or adults based on the EdgeR results.

Figure 6: Diverse Pf-malaria antigen-specific expression patterns of cT_{FH} defining cytokines and transcription factors for children. Heatmaps of Wilcoxon-paired two-tailed t-test *p*-values are shown for cT_{FH} meta-clusters comparing **(a)** *Pf*SEA-1A and **(b)** *Pf*-GARP versus unstimulated PBMCs from children (n=13) for each cytokine (IFNγ, IL4, and IL21) and transcription factor (Bcl6 and cMAF). The color-scale indicates the significance of the *p*-value: white (non-significant, $p>0.05$), yellow ($0.05>p>0.02$), orange ($0.02>p>0.005$), and red (highly significant, $p<0.005$). The down-directed arrow indicates a decrease of expression

from unstimulated to stimulated condition whereas no arrow indicates an increase of expression from unstimulated to stimulated condition. The cT_{FH} meta-clusters that co-expressed transcription factors were grouped as follows: Group 1 (blue line), Group 2 (green line), and Group 3 (purple line). Bar plots indicating mean with SD of the median intensity fluorescence (MFI) of **(c)** IFNγ, **(d)** Bcl6, and **(e)** cMAF for the cT_{FH} meta-clusters showing significant statistical differences between *Pf*SEA-1A and *Pf*GARP stimulations. *p*-values from Wilcoxon-paired two-tailed t-tests are indicated.

Figure 7: Limited Pf-malaria antigen-specific expression patterns of cT_{FH} defining cytokines and transcription factors for adults. Heatmaps of Wilcoxon-paired two-tailed t-test *p*-values are shown for cT_{FH} meta-clusters comparing **(a)** *Pf*SEA-1A or **(b)** *Pf*-GARP versus unstimulated PBMCs from adults (n=13) for each cytokine (IFNγ, IL4, and IL21) and transcription factors (Bcl6 and cMAF). The color-scale indicates the significance of the *p*-value: white (non-significant, $p>0.05$), yellow ($0.05>p>0.02$), orange ($0.02>p>0.005$) and red (highly significant, $p<0.005$). The down-directed arrow indicates a decrease of expression from unstimulated to stimulated condition whereas no arrow indicates an increase of expression from unstimulated to stimulated condition. The only cT_{FH} meta-clusters that expressed transcription factors were in Group 3 (purple box). Bar plots indicating mean with SD of the median intensity fluorescence (MFI) of **(c)** Bcl6, and (**d**) cMAF for the cT_{FH} meta-clusters showing significant statistical differences between *Pf*SEA-1A and *Pf*GARP stimulations. *p*-values from Wilcoxon-paired two-tailed t-tests are indicated.

Figure 8: Abundance of cT_{FH} meta-clusters stratified by anti-PfGARP IgG antibody levels. UMAP and EdgeR analysis of **(a)** children (n=13) and **(b)** adults (n=13) where significant differences ($p<0.05$) in the abundance of the cT_{FH} meta-clusters are circled on high versus low PfGARP antibody level (left to right) UMAP and green dots on the volcano plot (far right).

Figure 9: Summary. Illustration of combined findings showing remarkable differences in cT_{FH} subset abundance and *Pf*-malaria antigen-specific cytokine and transcription factor responses between children and adults residing in a malaria holoendemic region of Kenya. Made with BioRender.

Figures

Figure_1:

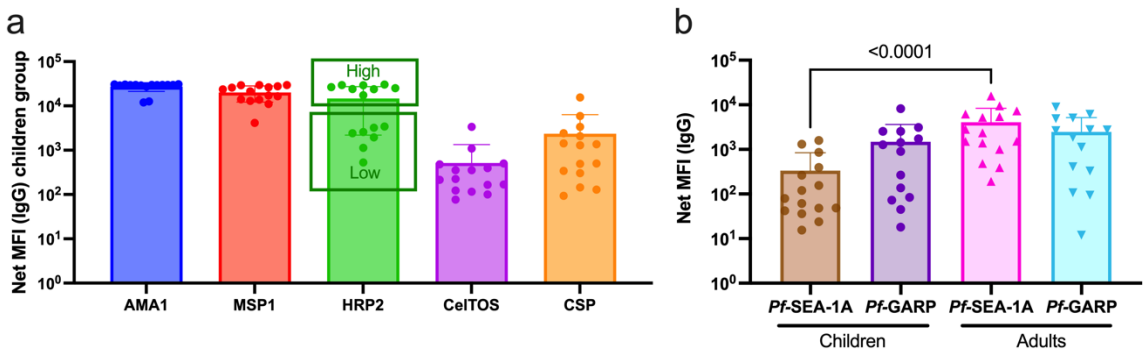

941

Figure_2:

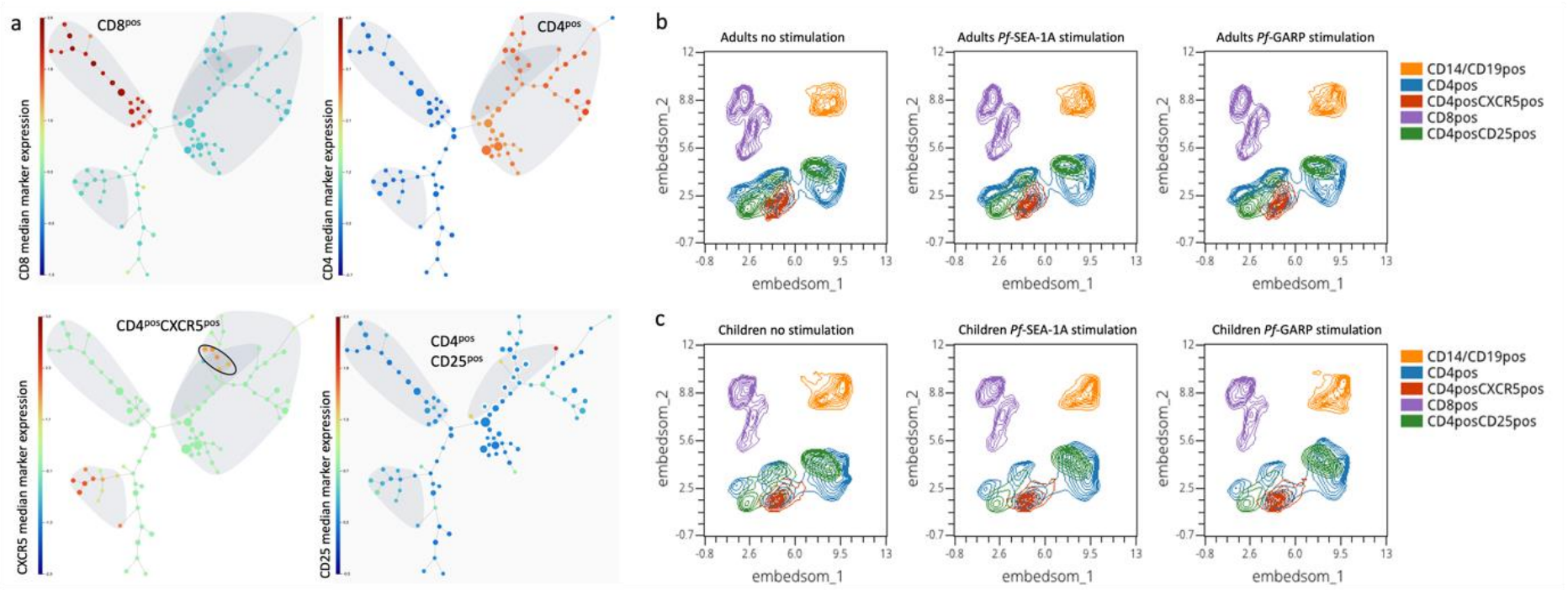
a
CD8pos
CD8 median marker expression
CD4pos
CD4 median marker expression
CD4posCXCR5pos
CXCR5 median marker expression
CD4pos
CD25pos
CD25 median marker expression
b
Adults no stimulation
Adults Pf-SEA-1A stimulation
Adults Pf-GARP stimulation
c
Children no stimulation
Children Pf-SEA-1A stimulation
Children Pf-GARP stimulation
embedsom_1
embedsom_2
CD14/CD19pos
CD4pos
CD4posCXCR5pos
CD8pos
CD4posCD25pos

Figure_3:

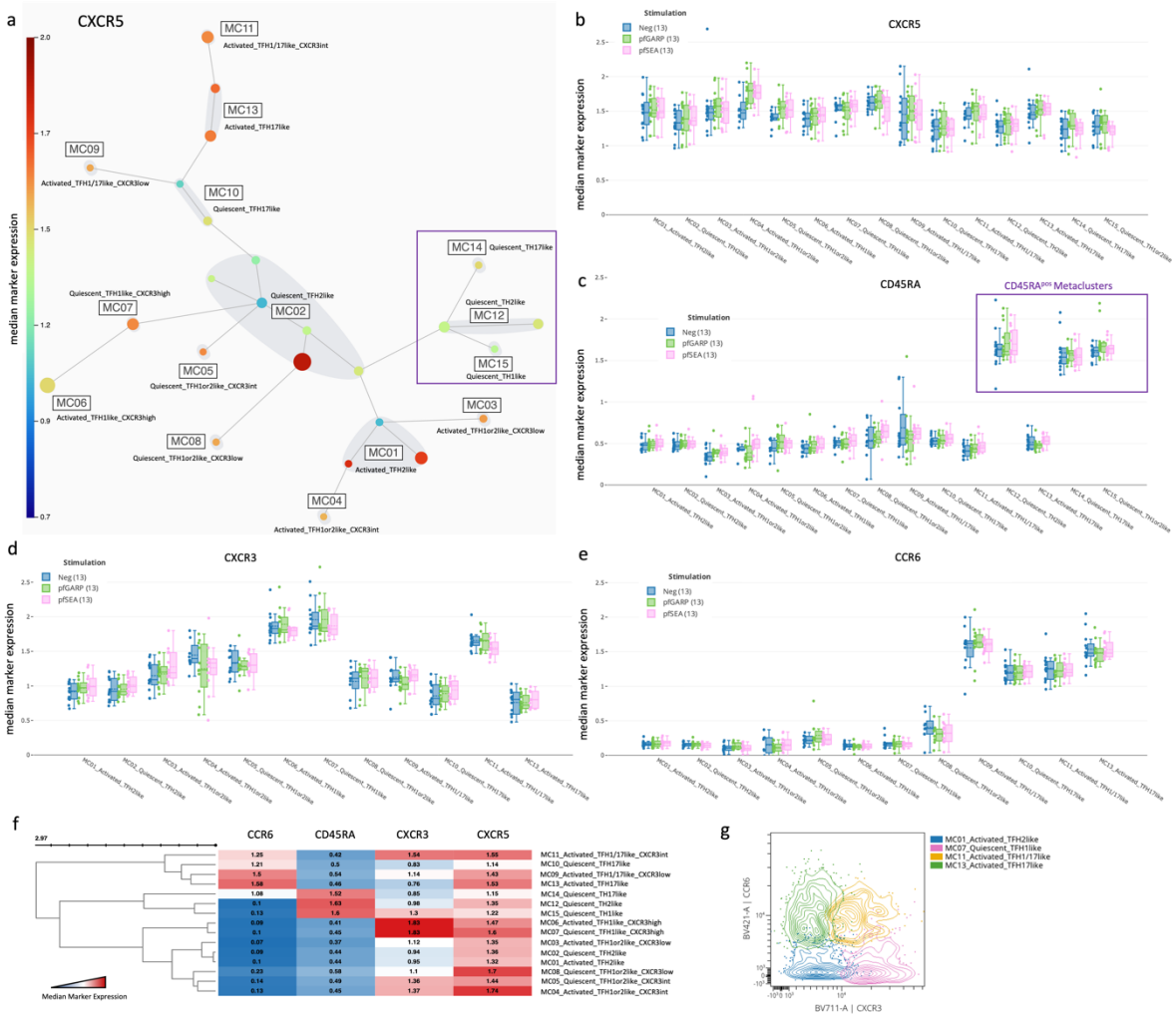
a
CXCR5
median marker expression
MC11
Activated_TFH1/17like_CXCR3int
MC13
Activated_TFH17like
MC09
Activated_TFH1/17like_CXCR3low
MC10
Quiescent_TFH17like
MC14
Quiescent_TH17like
Quiescent_TFH1like_CXCR3high
MC07
Quiescent_TFH2like
MC02
Quiescent_TH2like
MC12
MC15
Quiescent_TH1like
MC05
Quiescent_TFH1or2like_CXCR3int
MC06
Activated_TFH1like_CXCR3high
MC03
Activated_TFH1or2like_CXCR3low
MC08
Quiescent_TFH1or2like_CXCR3low
MC01
Activated_TFH2like
MC04
Activated_TFH1or2like_CXCR3int
b
CXCR5
Stimulation
Neg (13)
pfGARP (13)
pfSEA (13)
c
CD45RA
CD45RA^POS Metaclusters
d
CXCR3
e
CCR6
f
CCR6
CD45RA
CXCR3
CXCR5
Median Marker Expression
g
MC01_Activated_TFH2like
MC07_Quiescent_TFH1like
MC11_Activated_TFH1/17like
MC13_Activated_TFH17like
BV421-A | CCR6
BV711-A | CXCR3

Figure_4:

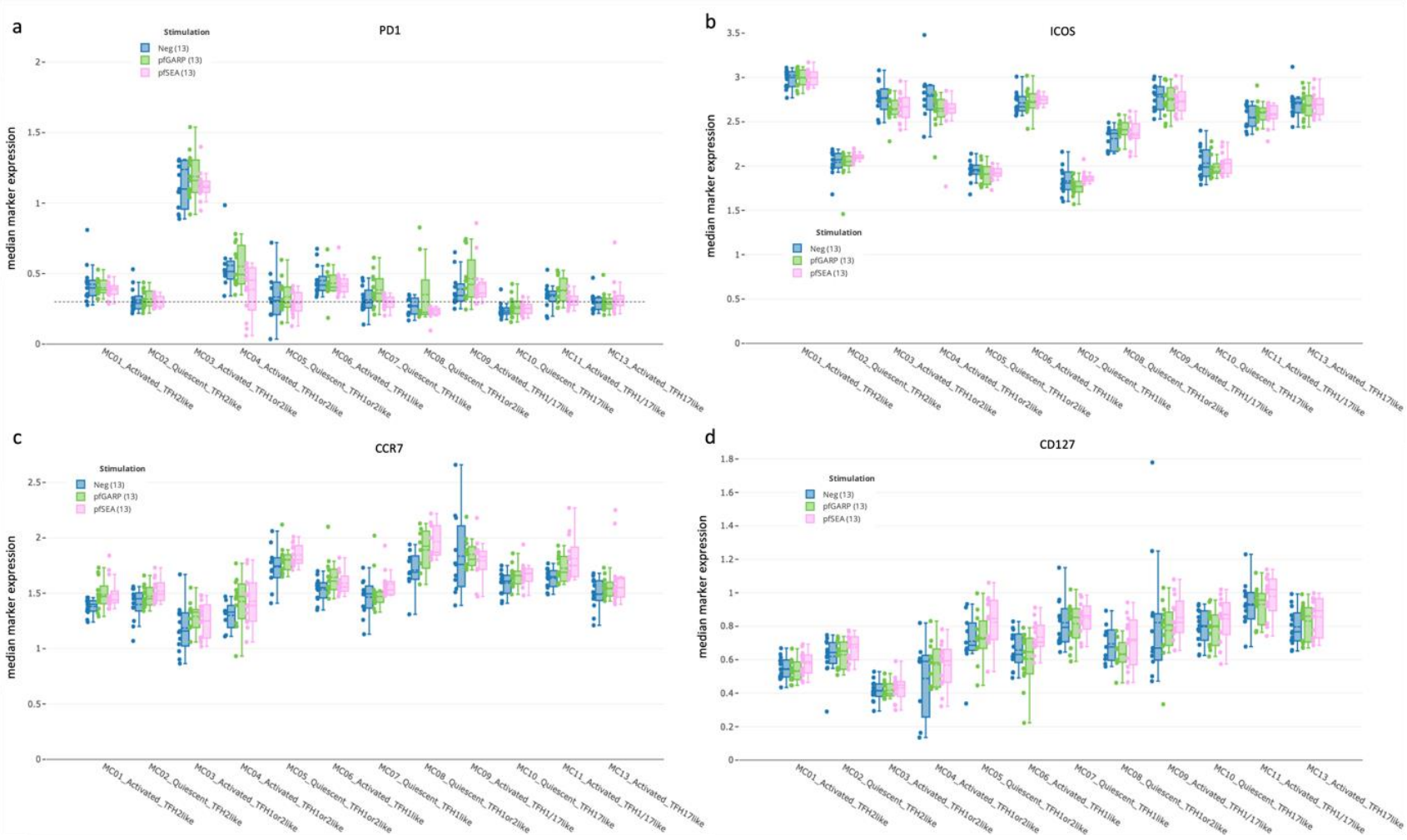
a
PD1
b
ICOS
c
CCR7
d
CD127
Stimulation
Neg (13)
pfGARP (13)
pfSEA (13)
median marker expression
MC01_Activated_TFH2like
MC02_Quiescent_TFH2like
MC03_Activated_TFH1or2like
MC04_Activated_TFH1or2like
MC05_Quiescent_TFH1or2like
MC06_Activated_TFH1like
MC07_Quiescent_TFH1like
MC08_Quiescent_TFH1or2like
MC09_Activated_TFH1/17like
MC10_Quiescent_TFH17like
MC11_Activated_TFH1/17like
MC13_Activated_TFH17like

Figure_5:

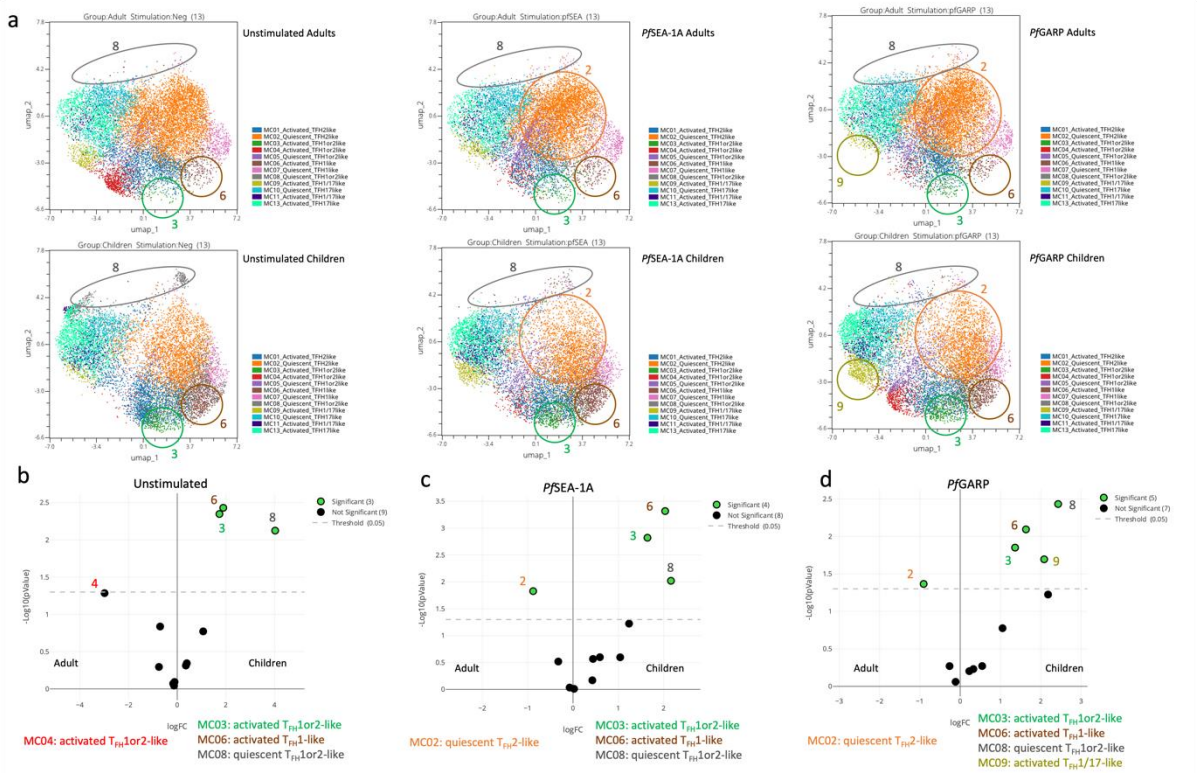

e

	MC01-Act TFH2like	MC02_Qui TFH2like	MC03_Act TFH1or2like	MC04_Act TFH1or2like	MC05_Qui TFH1or2like	MC06_Act TFH1like	MC07_Qui TFH1like	MC08_Qui TFH1or2like	MC09_Act TFH1/17like	MC10_Qui TFH17like	MC11_Act TFH1/17like	MC13_Act TFH17like	Abundance (% of total CD4pos CXCR5pos cells)
Neg	13.4	41.2	0.96	5.48	1.89	2.08	3.42	0.45	2.64	9.18	1.45	7.49	concat_Adult
	16.2	24.1	3.39 *	0.58	1.52	6.64 *	2.88	7.47 *	1.32	8.17	2.88	9.58	concat_Children
PfSEA-1A	13.3	40.9 *	0.94	5.48	1.9	2.02	3.38	0.45	2.65	8.71	1.48	7.85	concat_Adult
	16.3	24.4	3.42 *	0.58	1.52	6.7 *	2.92	7.46 *	1.3	8.65	2.85	9.22	concat_Children
PfGARP	14.8	35.7 *	1.46	5.66	2.12	3.2	3.63	0.63	2.92	8.04	1.72	7.56	concat_Adult
	14.8	29.5	2.89 *	0.4	1.3	5.52 *	2.66	7.28 *	1.04 *	9.32	2.62	9.52	concat_Children

Figure_6:

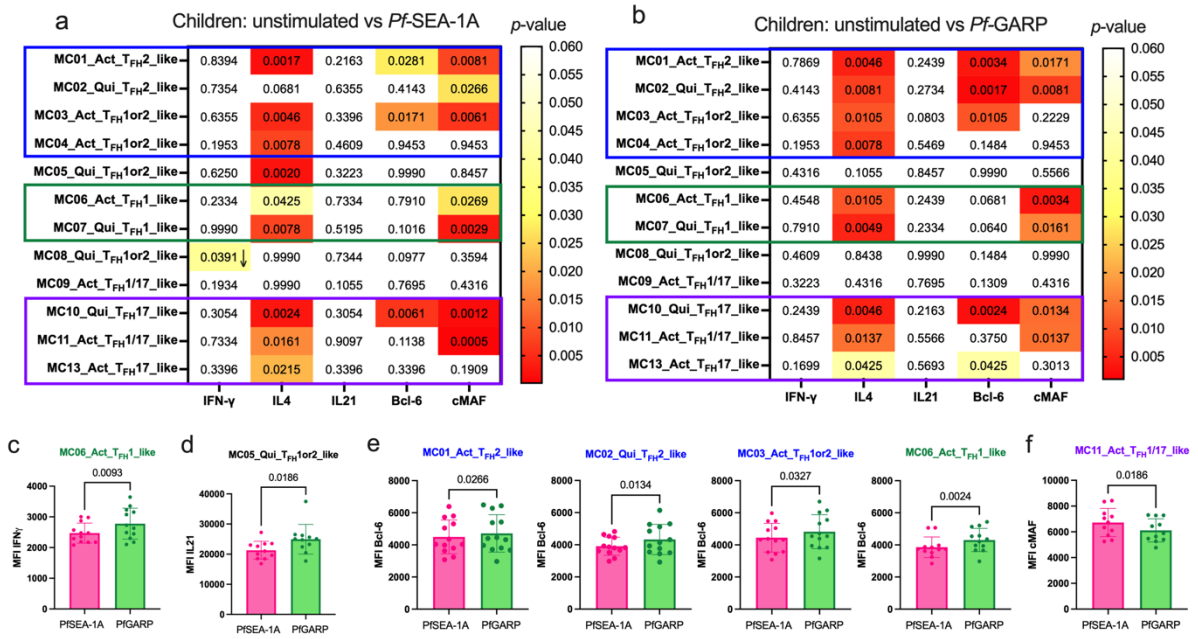

Figure_7:

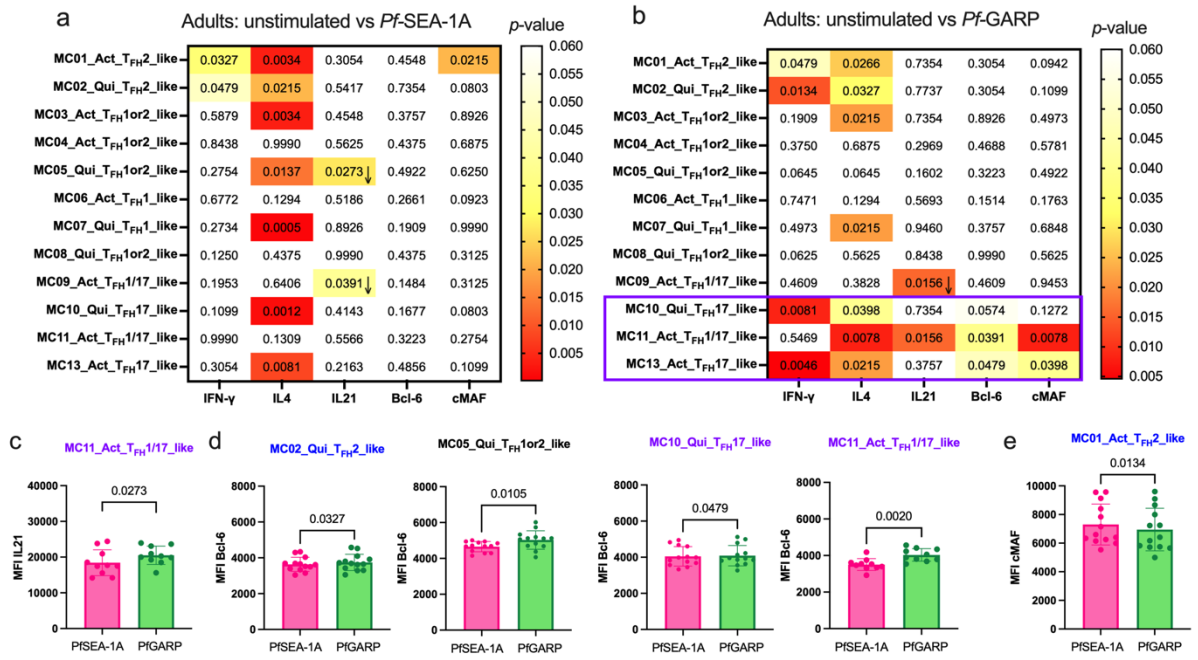

Figure_8:

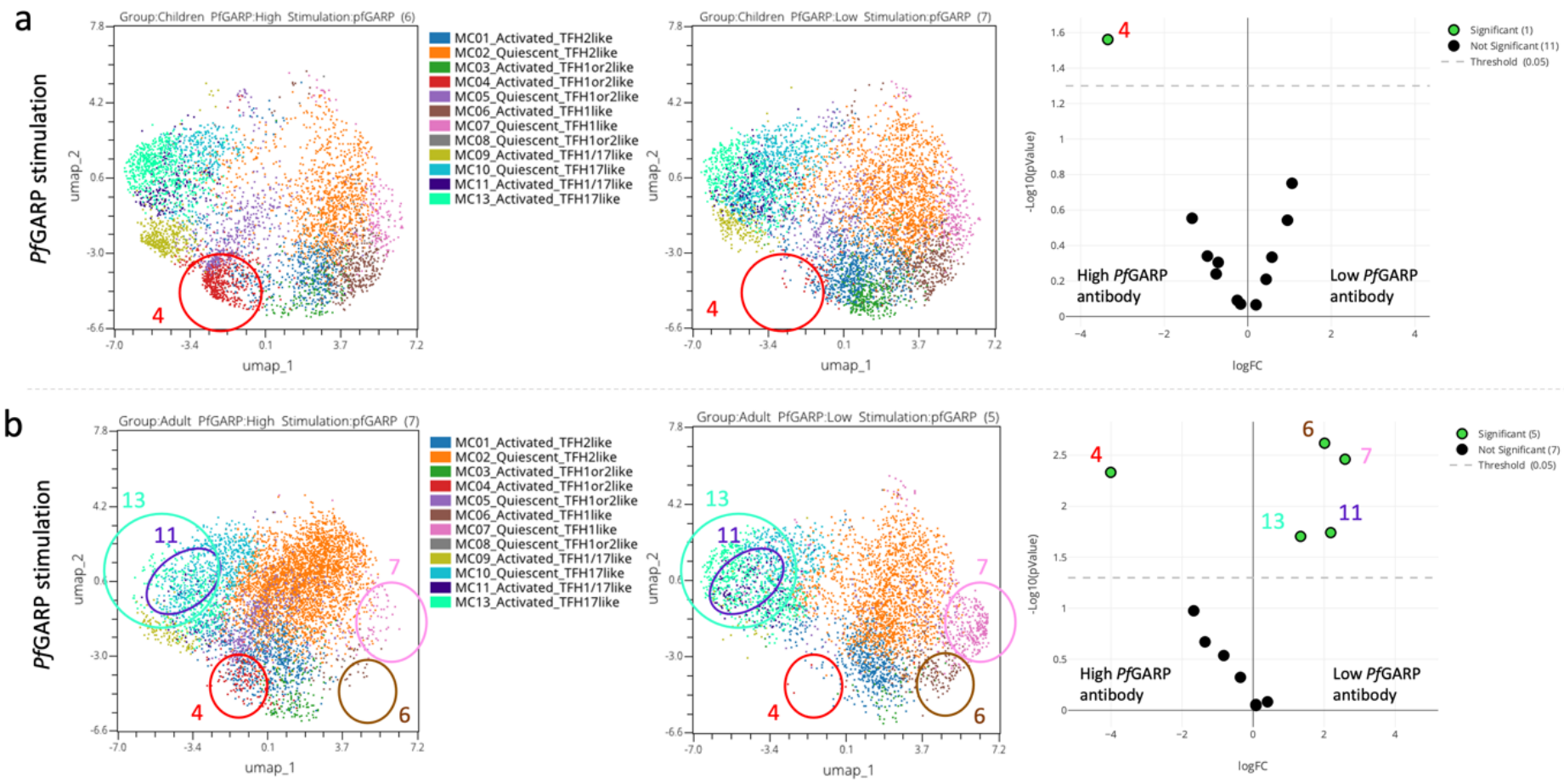
a
PfGARP stimulation
Group:Children PfGARP:High Stimulation:pfGARP (6)
Group:Children PfGARP:Low Stimulation:pfGARP (7)
MC01_Activated_TFH2like
MC02_Quiescent_TFH2like
MC03_Activated_TFH1or2like
MC04_Activated_TFH1or2like
MC05_Quiescent_TFH1or2like
MC06_Activated_TFH1like
MC07_Quiescent_TFH1like
MC08_Quiescent_TFH1or2like
MC09_Activated_TFH1/17like
MC10_Quiescent_TFH17like
MC11_Activated_TFH1/17like
MC13_Activated_TFH17like
umap_1
umap_2
Significant (1)
Not Significant (11)
Threshold (0.05)
-Log10(pValue)
logFC
High PfGARP antibody
Low PfGARP antibody
b
Group:Adult PfGARP:High Stimulation:pfGARP (7)
Group:Adult PfGARP:Low Stimulation:pfGARP (5)
Significant (5)
Not Significant (7)

Figure_9:

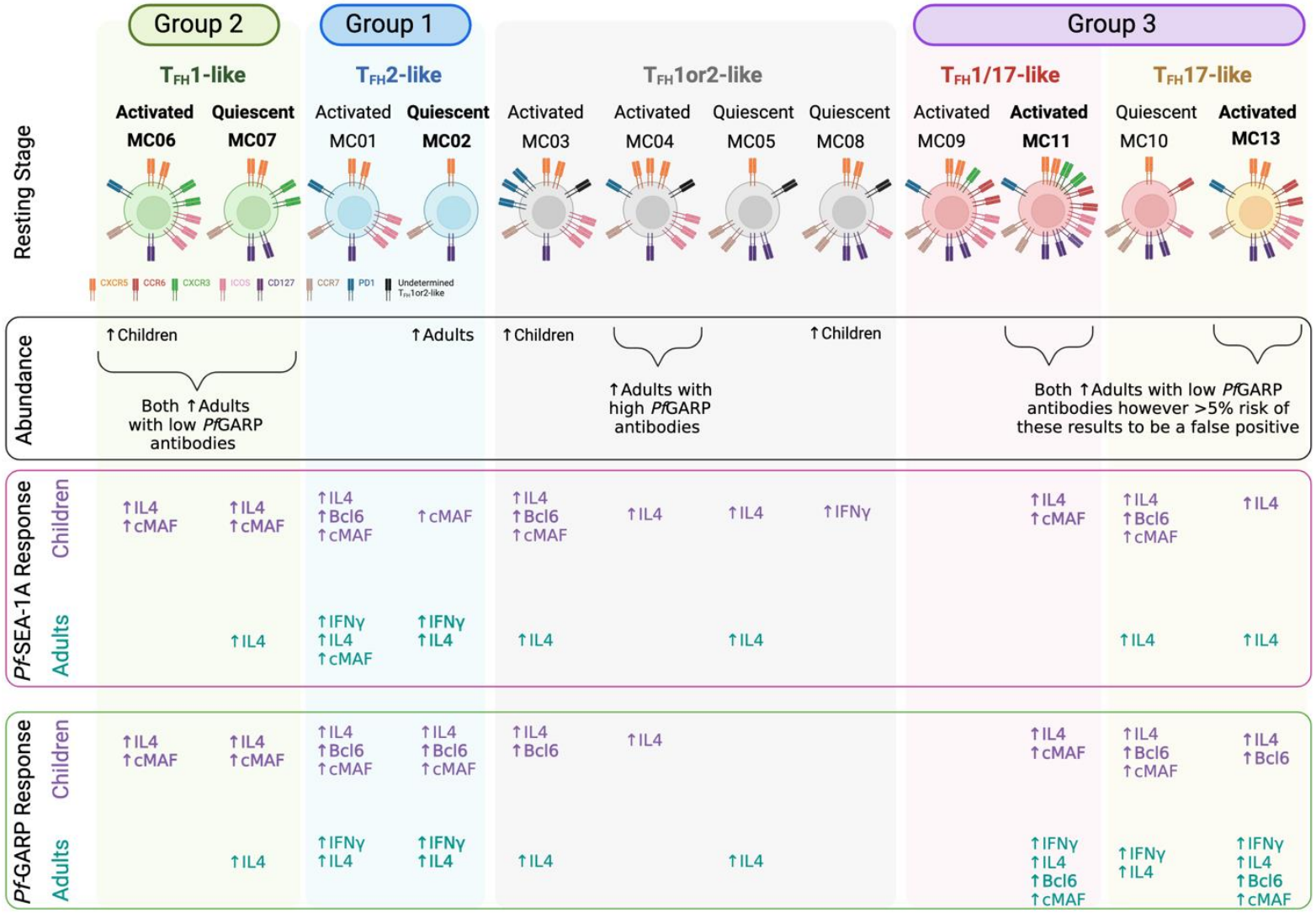
Group 2
Group 1
Group 3
TFH1-like
TFH2-like
TFH1or2-like
TFH1/17-like
TFH17-like
Activated MC06
Quiescent MC07
Activated MC01
Quiescent MC02
Activated MC03
Activated MC04
Quiescent MC05
Quiescent MC08
Activated MC09
Activated MC11
Quiescent MC10
Activated MC13
Resting Stage
CXCR5 CCR6 CXCR3 ICOS CD127
CCR7 PD1 Undetermined TFH1or2-like
Abundance
↑Children
↑Adults
↑Children
↑Children
Both ↑Adults with low PfGARP antibodies
↑Adults with high PfGARP antibodies
Both ↑Adults with low PfGARP antibodies however >5% risk of these results to be a false positive
Pf-SEA-1A Response
Children
↑IL4 ↑cMAF
↑IL4 ↑cMAF
↑IL4 ↑Bcl6 ↑cMAF
↑cMAF
↑IL4 ↑Bcl6 ↑cMAF
↑IL4
↑IL4
↑IFNγ
↑IL4 ↑cMAF
↑IL4 ↑Bcl6 ↑cMAF
↑IL4
Adults
↑IL4
↑IFNγ ↑IL4 ↑cMAF
↑IFNγ ↑IL4
↑IL4
↑IL4
↑IL4
↑IL4
Pf-GARP Response
Children
↑IL4 ↑cMAF
↑IL4 ↑cMAF
↑IL4 ↑Bcl6 ↑cMAF
↑IL4 ↑Bcl6 ↑cMAF
↑IL4 ↑Bcl6
↑IL4
↑IL4 ↑cMAF
↑IL4 ↑Bcl6 ↑cMAF
↑IL4 ↑Bcl6
Adults
↑IL4
↑IFNγ ↑IL4
↑IFNγ ↑IL4
↑IL4
↑IL4
↑IFNγ ↑IL4 ↑Bcl6 ↑cMAF
↑IFNγ ↑IL4
↑IFNγ ↑IL4 ↑Bcl6 ↑cMAF

Supplementals

Supplemental_Figure_1:

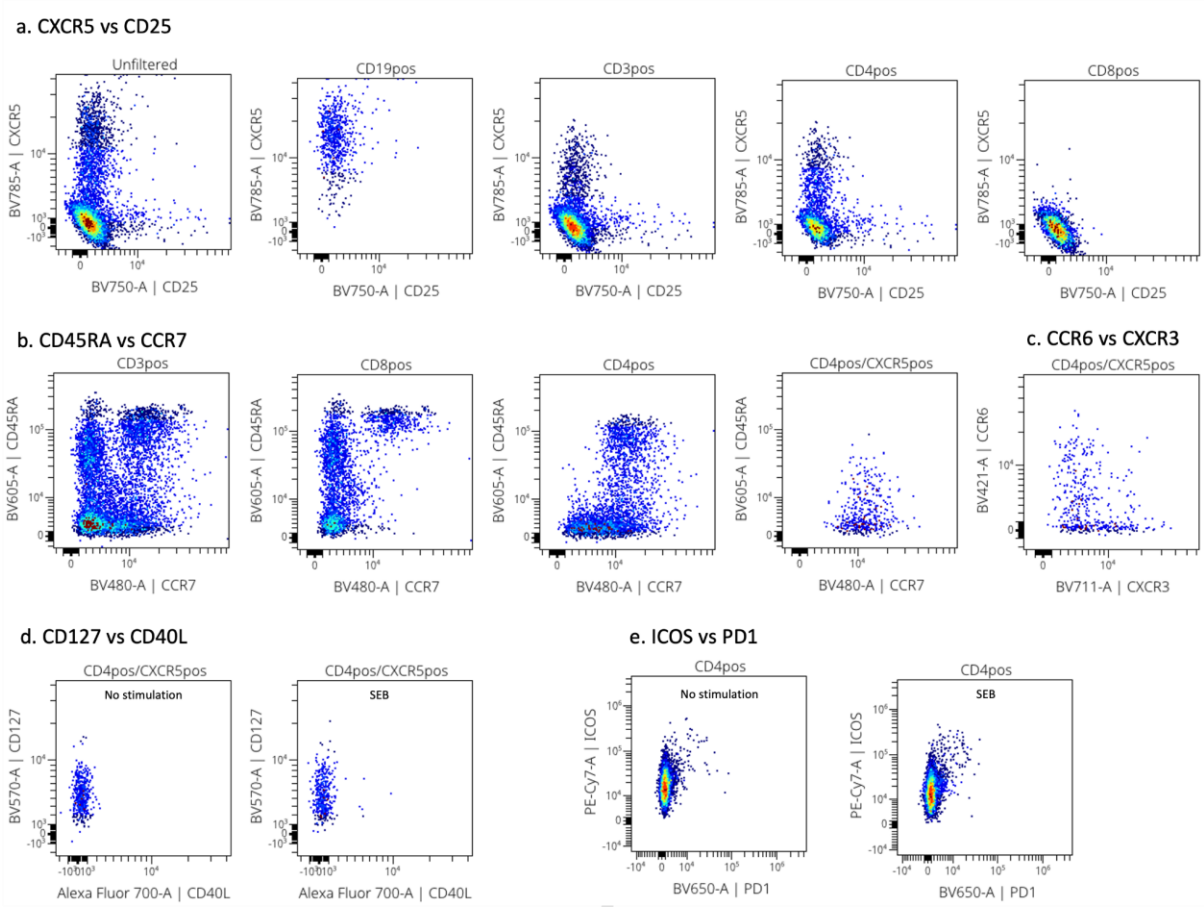

Supplemental Figure 1: Representative cytoplots of the extracellular flow staining. Panel **a** shows the CXCR5 vs CD25 cytoplots on unfiltered, CD19^{pos}, CD3^{pos}, CD4^{pos} and CD8^{pos} cells from left to right. Panel **b** shows CD45RA vs CCR7 cytoplots on CD3^{pos}, CD8^{pos}, CD4^{pos} and CD4^{pos}CXCR5^{pos} cells from left to right. Panel **c** shows CCR6 vs CXCR3 staining on CD4^{pos}CXCR5^{pos} cells. Panel **d** shows CD127 vs CD40L expression within CD4^{pos}CXCR5^{pos} cells by unstimulated and SEB stimulated cells. Panel **e** shows ICOS vs PD1 cytoplots after no stimulation or SEB 6h stimulation.

Supplemental_Figure_2:

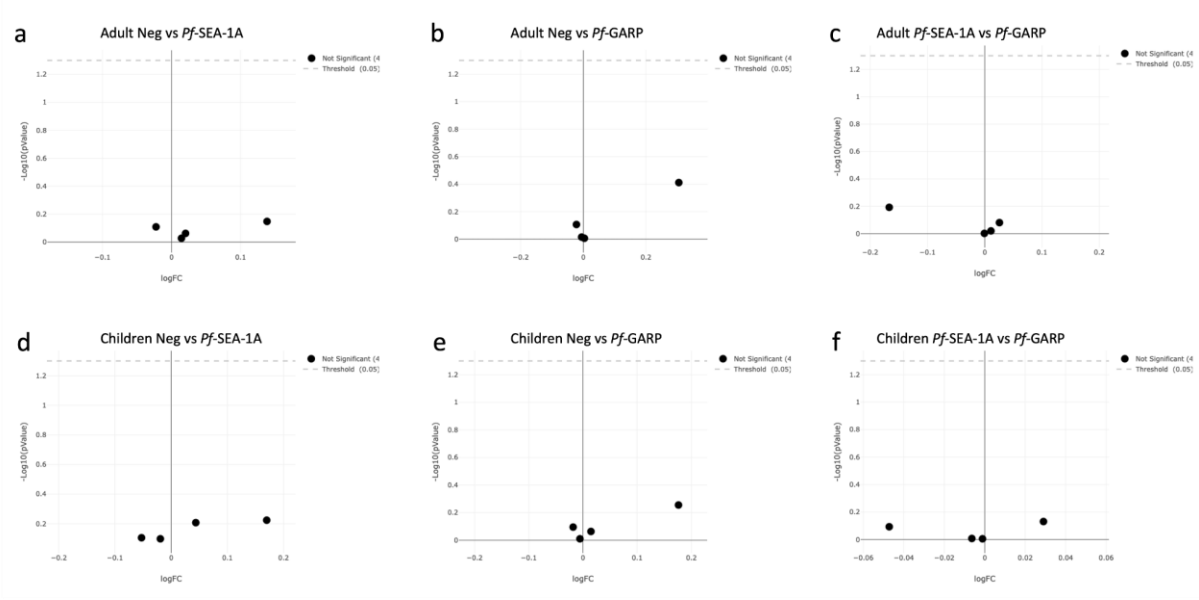

Supplemental Figure 2: EdgeR analysis of the CD4^{pos}, CD4^{pos}CXCR5^{pos}, CD8^{pos} and CD14/CD19^{pos} populations under different stimulation conditions in adults (n=15) and children (n=14). Volcano plot from EdgeR analysis comparing CD4^{pos}, CD4^{pos}CXCR5^{pos}, CD8^{pos}, and CD14/CD19^{pos} populations from adult PBMCs under the following conditions: **(a)** unstimulated versus *Pf*SEA-1A, **(b)** unstimulated versus *Pf*GARP, and **(c)** *Pf*SEA-1A versus *Pf*GARP. Volcano plot from EdgeR analysis comparing CD4^{pos}, CD4^{pos}CXCR5^{pos}, CD8^{pos},and CD14/CD19^{pos} populations from children PBMCs under the following conditions: **(d)** unstimulated versus *Pf*SEA-1A, **(e)** unstimulated versus *Pf*GARP, and **(f)** *Pf*SEA-1A versus *Pf*GARP. The green dots are statistically significant whereas the black dots are not, here no green dots were observed.

Supplemental_Figure_3:

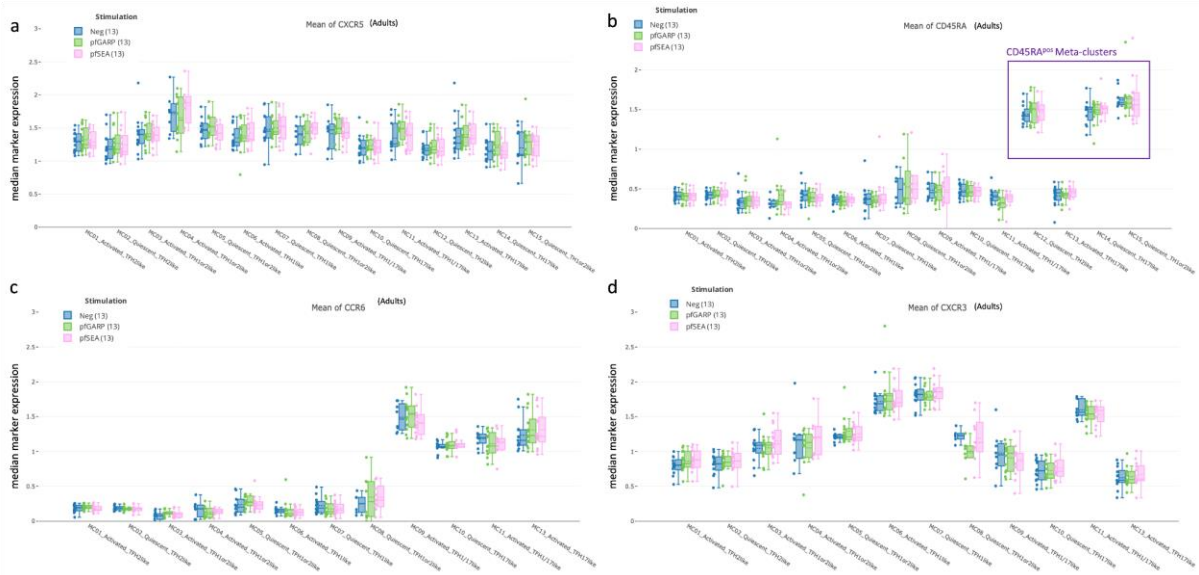

Supplemental Figure 3: Characterization of T_{FH} subsets using CXCR5, CXCR3, CCR6, and CD45RA expression. Bar plots showing **(a)** CXCR5, **(b)** CD45RA, **(c)** CCR6, and **(d)** CXCR3 expression across all cT_{FH}-like meta-clusters from adults (n=13) under no stimulation (blue), *Pf*GARP (green) and *Pf*SEA-1A (pink) stimulations. Fifty percent of the data are within the box limits, the solid line indicates the median, the dash line the mean and the whiskers indicate the range of the remaining data with outliers being outside that range.

Supplemental_Figure_4:

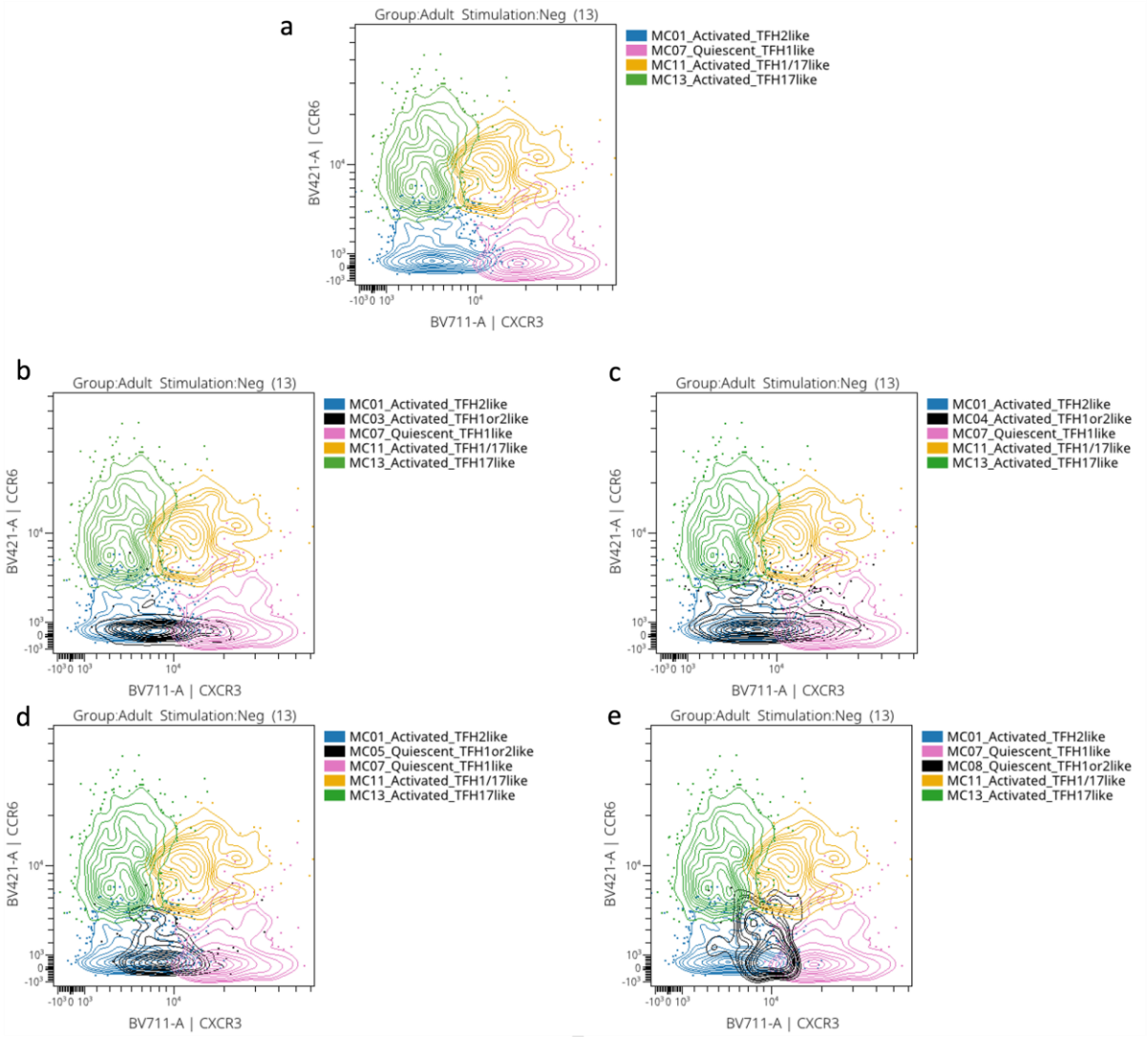

Supplemental Figure 4: CCR6 versus CXCR3 representative cytoplots. a. CCR6 vs CXCR3 expression from activated $cT_{FH}2$-like MC01 (in blue), quiescent $cT_{FH}1$-like MC07 (in pink), activated $cT_{FH}1/17$-like MC11 (in orange) and activated $cT_{FH}17$-like MC13 (in green). Undetermined meta-clusters was superposed to the sus-mentioned metacluster: activated $cT_{FH}1or2$-like MC03 (in black) (**b**); activated $cT_{FH}1or2$-like MC04 (in black) (**c**); quiescent $cT_{FH}1or2$-like MC05 (in black) (**d**); quiescent $cT_{FH}1or2$-like MC08 (in black) (**e**).

Supplemental_Figure_5:

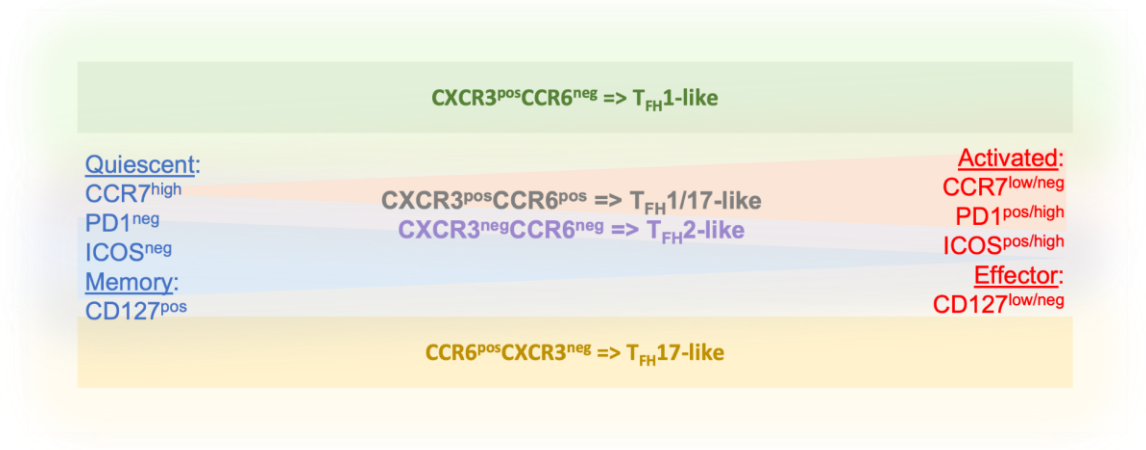

Supplemental Figure 5: Cartoon of T_{FH} subsets and their state of activation.

Supplemental_Figure_6:

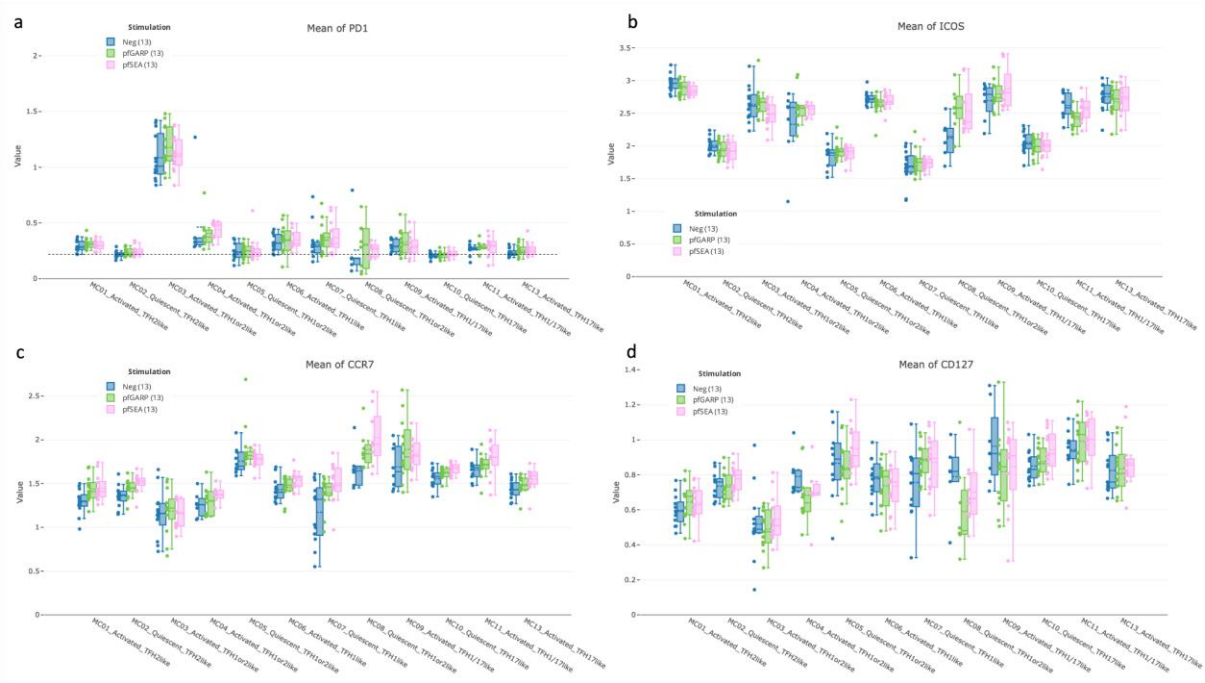

Supplemental Figure 6: State of activation of cT_{FH} subsets from adults determined by PD1, ICOS, CCR7, and CD127. Bar plots showing **(a)** PD1, **(b)** ICOS, **(c)** CCR7 and **(d)** CD127 expression across all cT_{FH}-like meta-clusters in adults (n=13) under no stimulation (blue), *Pf*GARP (green) and *Pf*SEA-1A (pink) stimulations. Fifty percent of the data are within the box limits, the solid line indicates the median, the dash line the mean and the whiskers indicate the range of the remaining data with outliers being outside that range.

Supplemental_Figure_7:

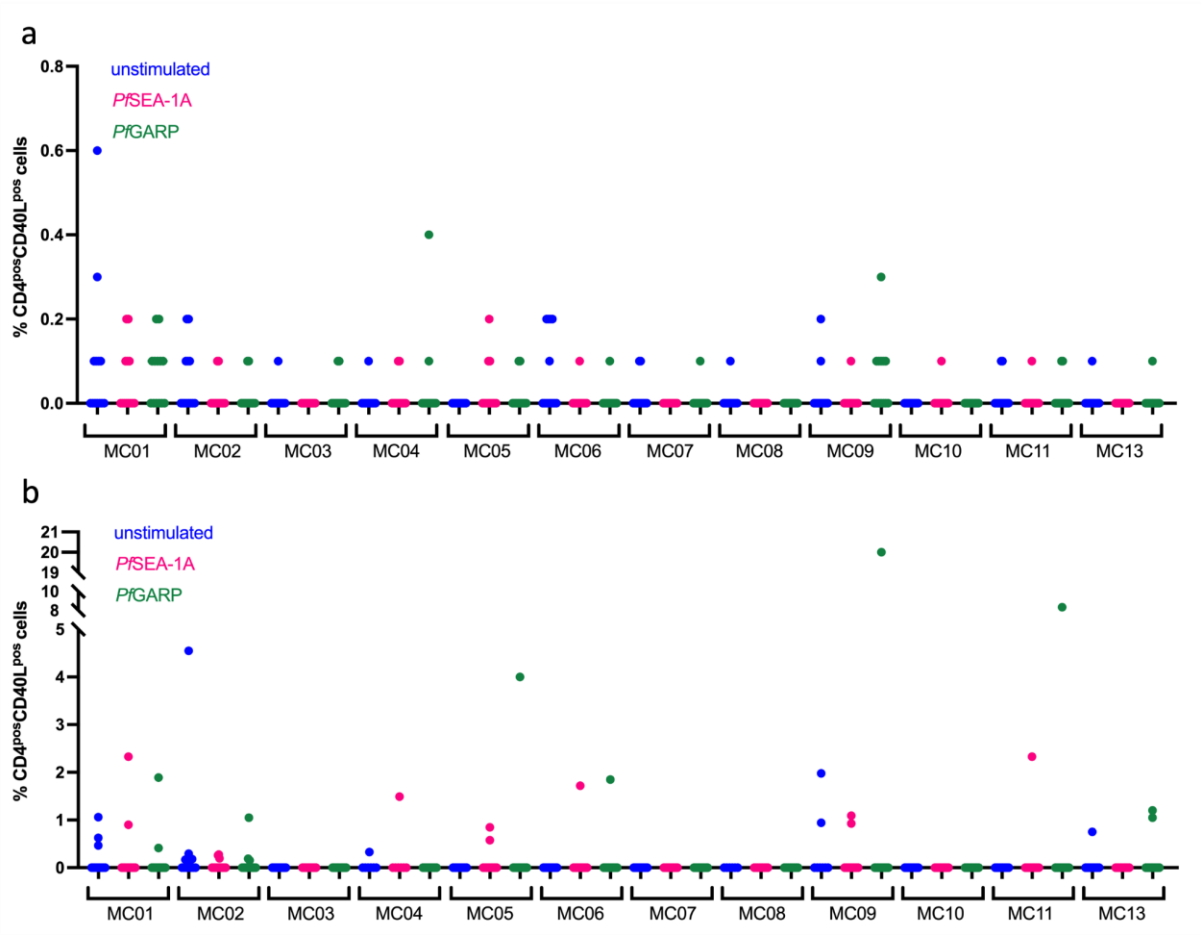

Supplemental Figure 7: CD40L expression across stimulation and meta-clusters. Dot plots of CD40L expression after manual gating based on unstimulated condition from children (n=13) (**a**) and adults (n=13) (**b**) cT_{FH} meta-clusters.

Supplemental_Figure_8:

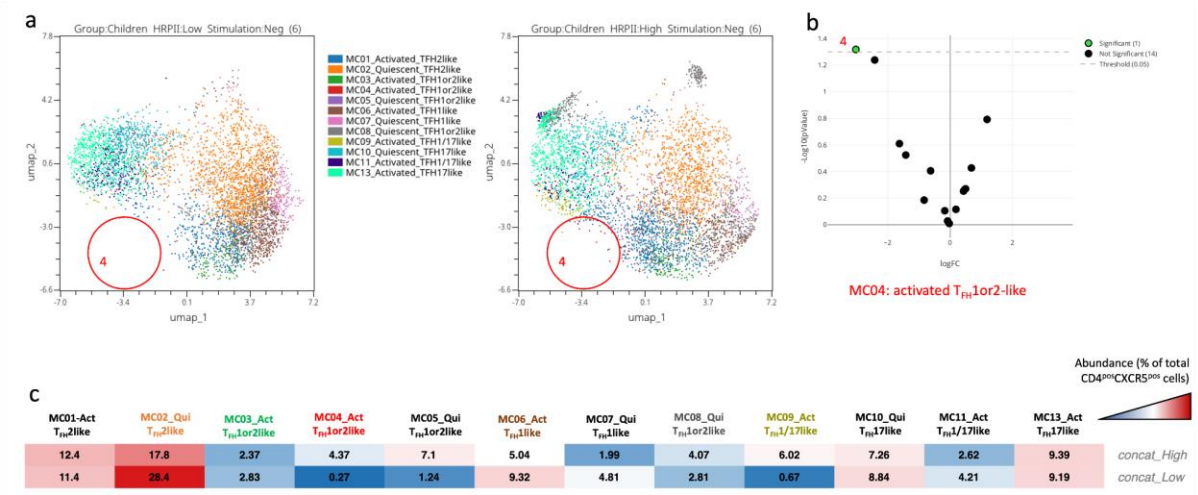

Supplemental Figure 8: Abundance of the cT_{FH} meta-clusters within children with low or high levels of HRP2 antibodies. (a) UMAP plot showing the clustering of the 13 different cT_{FH} meta-clusters (MC15) in children with low levels of HRP2 (on the left, n=6) and high levels of HRP2 (on the right, n=6) in the absence of stimulation. Each color represents a meta-cluster. The red circles highlight the meta-cluster showing differences in its abundance between the two groups of children. **(b)** An EdgeR statistical plot was performed to assess the abundance of the 13 meta-clusters between unstimulated PBMCs from both groups of children; the Y-axis being -log10(*p*-value) and the X-axis shows the log(FC). The green dot (MC04) is statistically significant whereas the black dots are not. **(c)** An abundance heatmap showing the distribution (in %) of each meta-cluster within the two groups of children (both concatenated unstimulated PBMCs from six participants). The color scale ranges from high abundance (red) to low abundance (blue).

Supplemental_Figure_9:

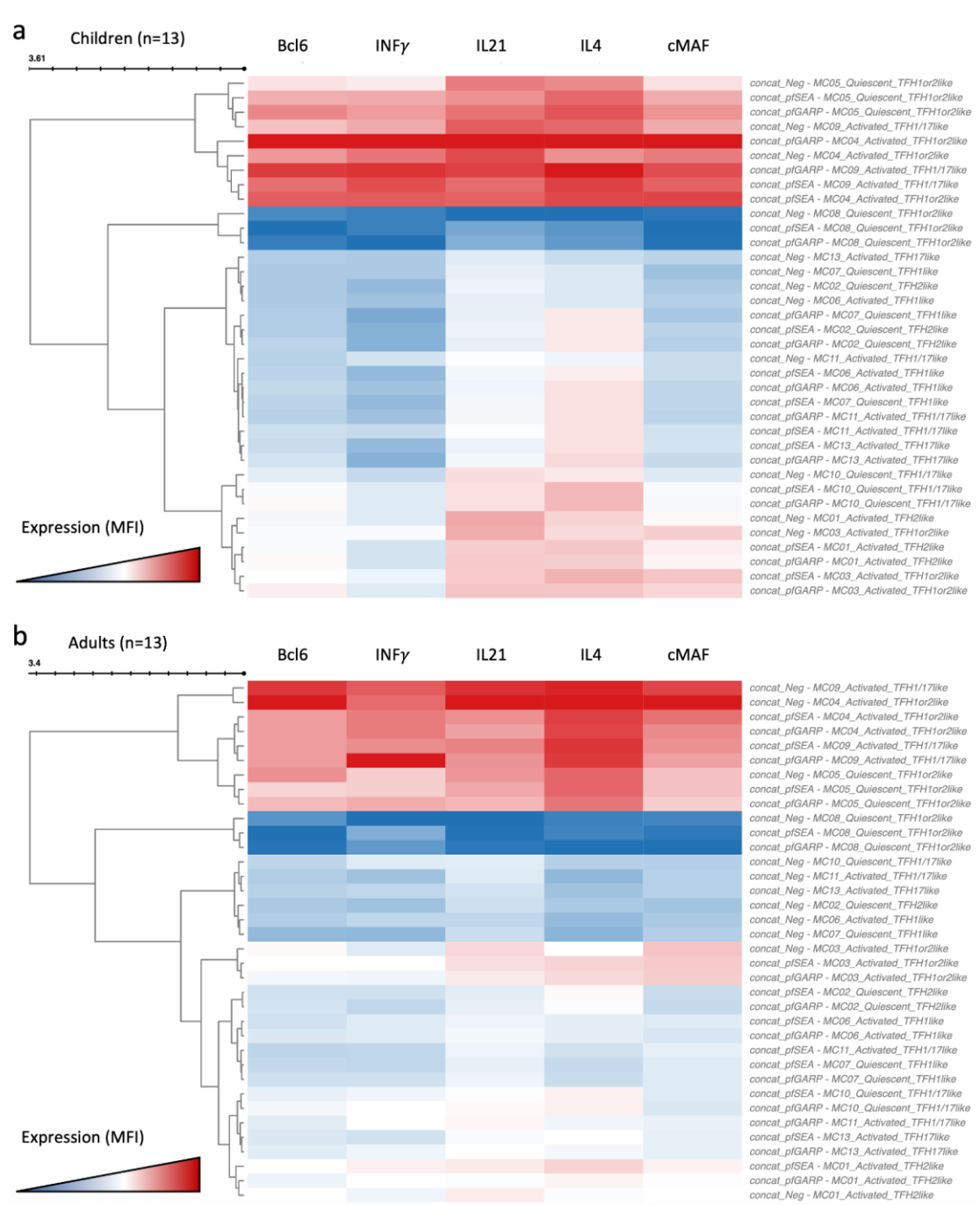

Supplemental Figure 9: Clustered heatmap of the cytokines and transcription factors expressed from cT_{FH} meta-clusters in adults and children under the different stimulation conditions. Heatmap of Bcl6, IFNγ, IL21, IL4, and cMAF expression from the 13 cT_{FH} meta-clusters from concatenated data from **(a)** children (n=13) and **(b)** adults (n=13), after stimulation by *Pf*SEA-1A or *Pf*GARP, or without any stimulation as indicated in the name of each row. The color scale ranges from high expression (red) to low/no expression (blue).

Supplemental_Figure_10:

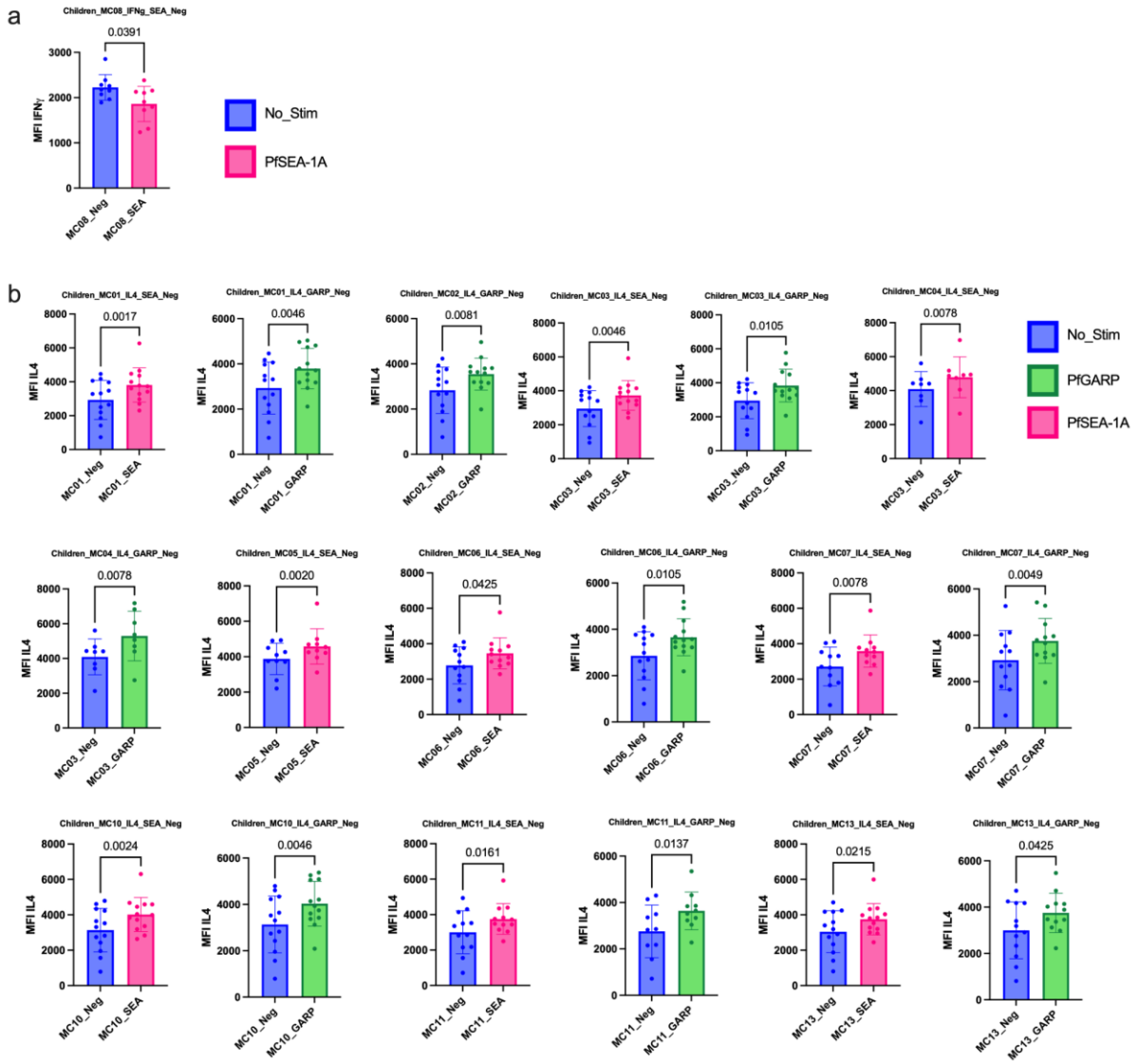

Supplemental Figure 10: Bar plots of cytokines expressed under the different conditions of stimulation in children (n=13). Comparison of mean fluorescent intensity (MFI) of **(a)** IFNγ, **(b)** IL4 cytokines expression after *Pf*SEA-1A (pink) or *Pf*GARP (green) stimulation or no stimulation control (blue). Bar plots indicate mean with SD. Wilcoxon-paired two-tailed t-tests were performed and *p*-values are indicated.

Supplemental_Figure_11:

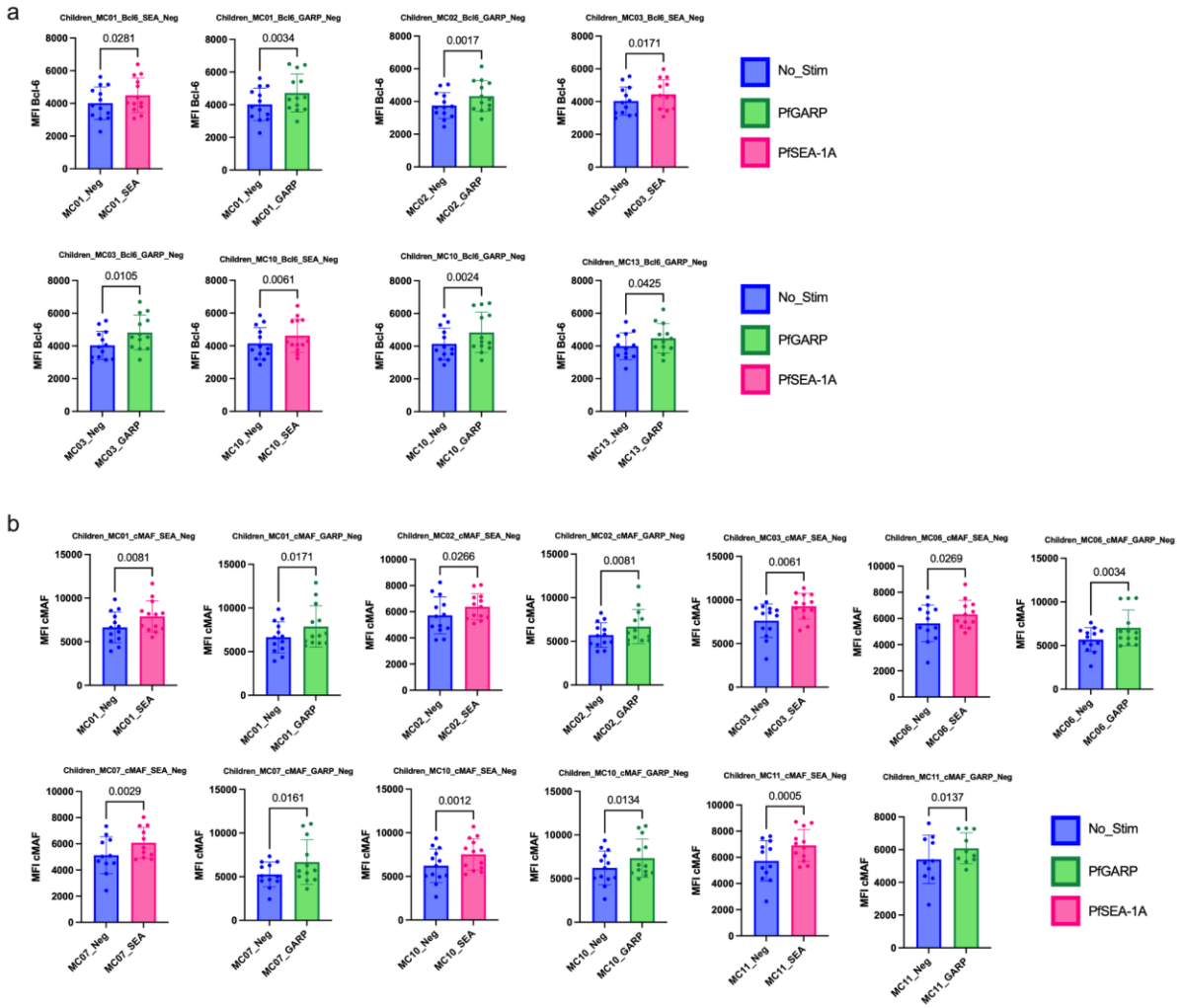

Supplemental Figure 11: Bar plots of transcription factors expressed under the different conditions of stimulation in children (n=13). Comparison of mean fluorescent intensity (MFI) of **(a)** Bcl6 and **(b)** cMAF expression after *Pf*SEA-1A (pink) or *Pf*GARP (green) stimulation or no stimulation control (blue). Bar plots indicate mean with SD. Wilcoxon-paired two-tailed t-tests were performed and *p*-values are indicated.

Supplemental_Figure_12:

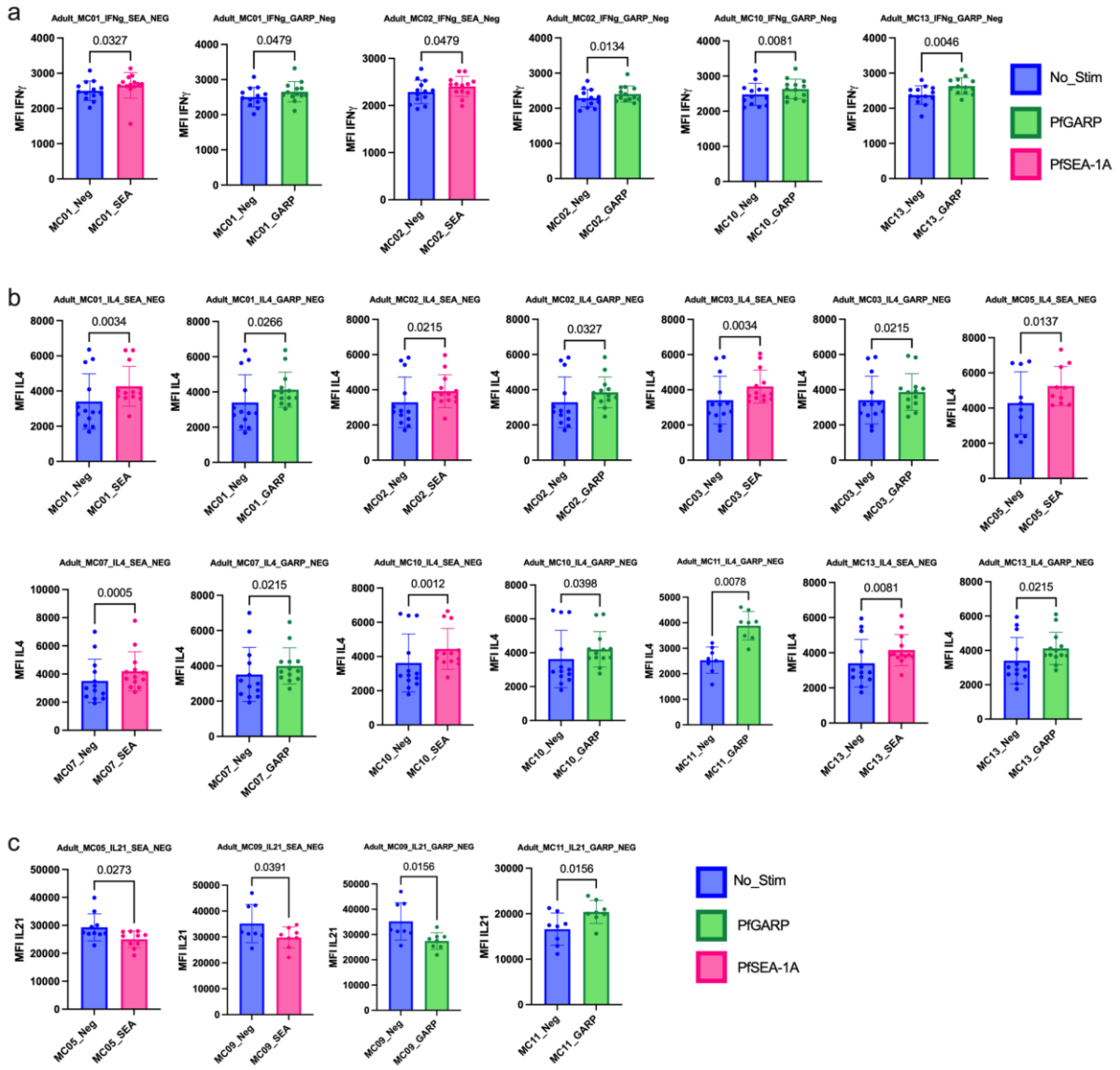

Supplemental Figure 12: Bar plots of cytokines expressed under the different conditions of stimulation in adults (n=13). Comparison of mean fluorescent intensity (MFI) of **(a)** IFNγ, **(b)** IL4 and **(c)** IL21 and cytokines expression after *Pf*SEA-1A (pink) or *Pf*GARP (green) stimulation or no stimulation control (blue). Bar plots indicate mean with SD. Wilcoxon-paired two-tailed t-tests were performed and *p*-values are indicated.

Supplemental_Figure_13:

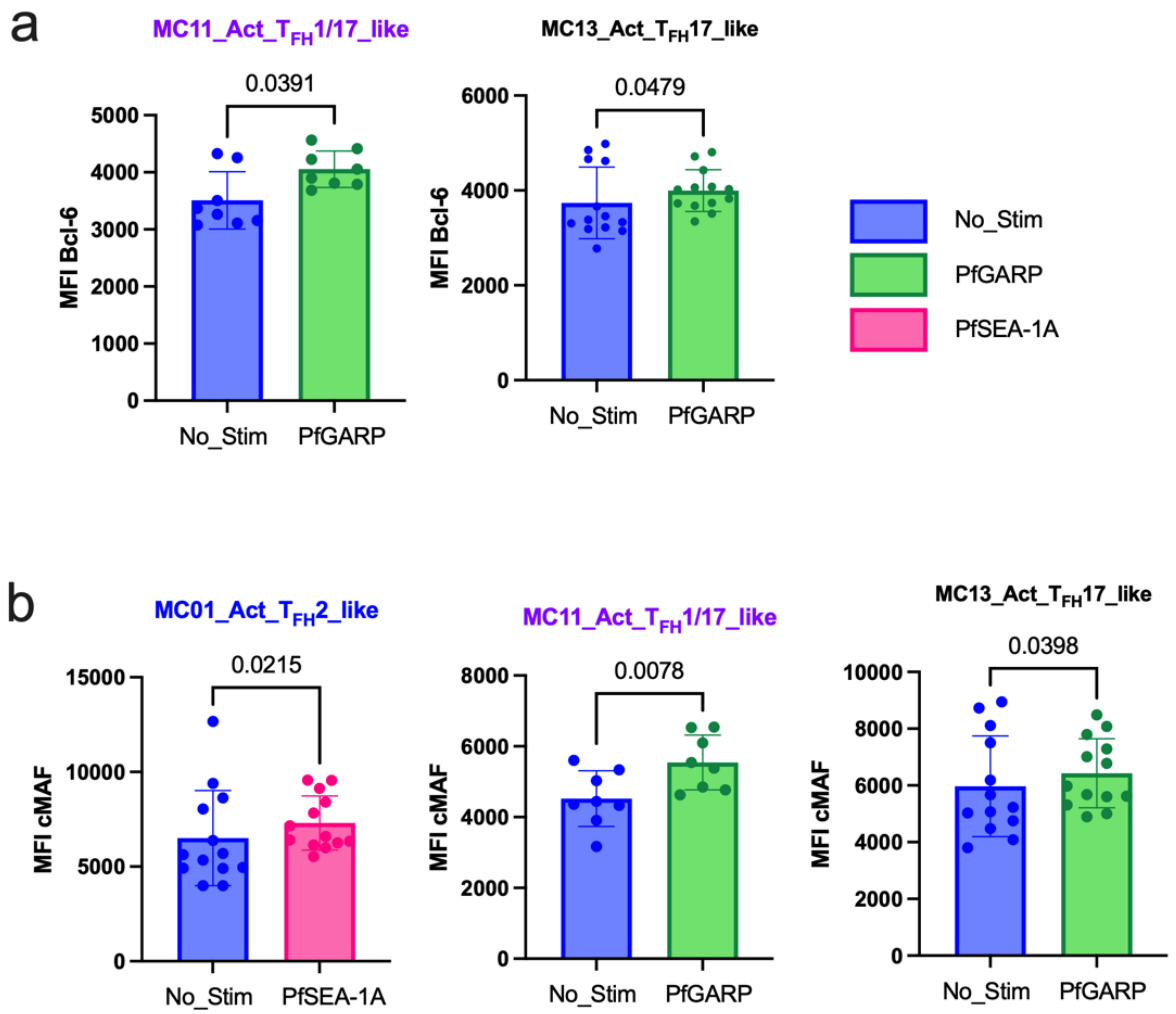

Supplemental Figure 13: Bar plots of transcription factors expressed under the different conditions of stimulation in adults (n=13). Comparison of mean fluorescent intensity (MFI) of **(a)** Bcl6 and **(b)** cMAF expression after *Pf*SEA-1A (pink) or *Pf*GARP (green) stimulation or no stimulation control (blue). Bar plots indicate mean with SD. Wilcoxon-paired two-tailed t-tests were performed and *p*-values are indicated.